Molecular and carbon isotopic geochemistry of crude oils and extracts from Permian source rocks in the northwestern and central Junggar Basin, China

Shuang Yu [a], Xulong Wang [b], Baoli Xiang [b], Jiangling Ren [b], Ertin Li [b], Jun Wang [a,c], Pan Huang [a], Guobin Wang [a], Hao Xu [a], Changchun Pan [a,*]

[a] State Key Laboratory of Organic Geochemistry, Guangzhou Institute of Geochemistry, Chinese Academy of Sciences, Wushan, Guangzhou 510640, China
[b] Xinjiang Oilfield Company, PetroChina, Karamay, Xinjiang 834000, China
[c] Shanghai Branch of CNOOC (China) Co Ltd, Shanghai 200030, China

ABSTRACT

The Junggar Basin is a major oil producing province in China. Most oil reservoirs found so far in this basin are in the Mahu sag and neighboring uplifts, northwestern Junggar Basin. A total of 78 oils and 10 Permian source rocks from the northwestern and central Junggar Basin and two oils and two Permian source rocks from the eastern Junggar Basin were analyzed by GC, GC–MS and GC–IRMS. The 78 oils can be clearly classified into two groups based on these analytical results. For group I oils, $\delta^{13}C$ values of individual *n*-alkanes are relatively higher and remain stable with increasing carbon number. For group II oils, these values are relatively lower and decrease at first, and then increase with carbon number. Differences in molecular parameters can be also observed between these two groups of oils. Group I oils generally have: (1) higher Pr/*n*-C_{17} and Ph/*n*-C_{18} ratios and lower Pr/Ph ratio, and (2) higher gammacerane/(C_{30} hopane + gammacerane) and β-carotane/(β-carotane + C_{30} hopane) ratios, compared with group II oils. In addition, group I oils mainly have tricyclic terpane distribution patterns with either $C_{20} < C_{21} < C_{23}$ and $C_{20} > C_{21} > C_{23}$ while group II oils mainly have the pattern of $C_{20} < C_{21}$ and $C_{21} > C_{23}$. However, molecular parameters overlap to some extent between these two groups of oils. Group I oils correlate well with the nine source rocks of the Lower Permian Fengcheng Formation (P_{1f}), while group II oils correlate well with the three source rocks of Middle Permian age based on carbon isotopic and molecular compositions. The occurrence of these two groups of oils in the northwestern and central Junggar Basin are consistent with facies and thickness variations in the source rocks within the Lower Permian Fengcheng Formation (P_{1f}) and Middle Permian Lower Wuerhe Formation (P_{2w}).

© 2017 Elsevier Ltd. All rights reserved.

1. Introduction

The Junggar Basin is a major oil producing province of China. Most oil reservoirs found so far in this basin are in Mahu sag and neighboring uplifts in the northwestern Junggar Basin (Fig. 1). The Karamay oil field in this region, discovered in 1955, was the first giant field found in China. Within and around the Mahu sag, total oil reserves proved in-place are up to 2×10^9 tonnes (e.g., Chen et al., 2013, 2014). In earlier studies, oils in this region were generally classified into two groups based on molecular parameters (Zhou et al., 1989; Yang et al., 1992). Group 1 oils are characterized by: (1) higher Pr/*n*-C_{17} and Ph/*n*-C_{18} ratios, (2) lower

relative concentrations, or even below the detection level of Ts, C_{29}Ts and C_{30} diahopane, and (3) high relative concentrations of gammacerane and carotanes. In contrast, group 2 oils are characterized by: (1) lower Pr/*n*-C_{17} and Ph/*n*-C_{18} ratios, (2) moderate and high relative concentrations of Ts, C_{29}Ts and C_{30} diahopane, and (3) moderate and lower relative concentrations of gammacerane and carotanes. The group 1 oils correlate with extracts of source rocks within the Lower Permian Fengcheng Formation (P_{1f}), while group 2 oils correlate with those within the Lower Permian Jiamuhe Formation (P_{1j}) below the Fengcheng Formation (P_{1f}) and the Middle Permian Lower Wuerhe Formation (P_{2w}) based on molecular parameters (Zhou et al., 1989; Yang et al., 1992; Zhang et al., 1993). Pan and Yang (2000) and Pan et al. (2003) documented the oil filling histories of oil reservoirs in the Junggar Basin based on these previous studies. In addition, Wang and Kang
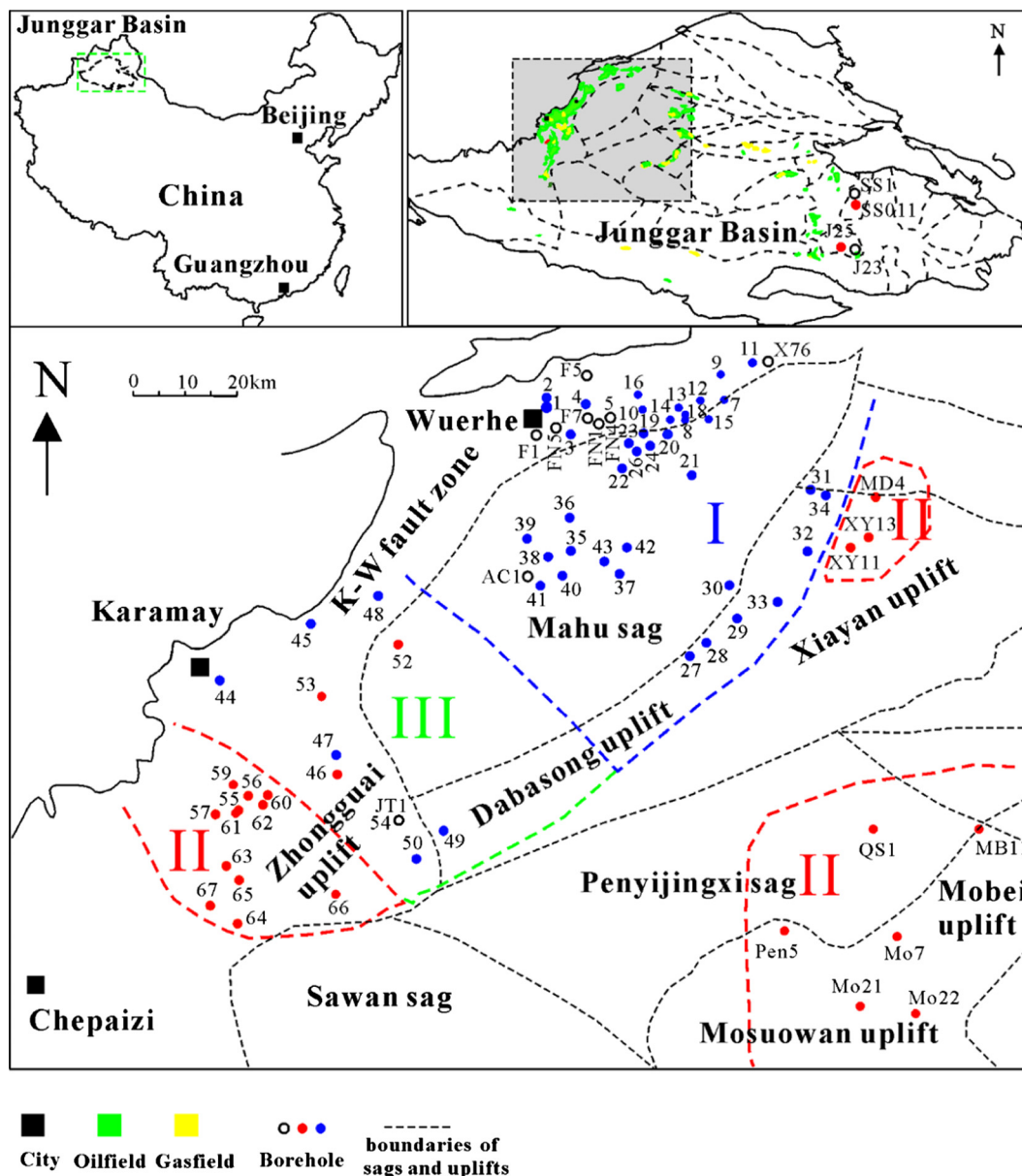
Fig. 1. Location map of the northwestern and central Junggar Basin and the sampled boreholes; 1–67 refer to oil numbers (same as in Table 2).

(1999, 2001) suggested that the tricyclic terpene distribution pattern is a critical indicator to determine the origins of oils in the northwestern and central Junggar Basin: the relative concentration sequences of tricyclic terpanes $C_{20} > C_{21} > C_{23}$ and $C_{20} < C_{21} < C_{23}$ are indicators of oils derived from source rocks within Lower Permian Jiamuhe (P_{1j}) and Lower Permian Fengcheng (P_{1f}) formations, respectively while the pattern $C_{20} < C_{21}$ and $C_{21} > C_{23}$ is an indicator for source rocks within the Middle Permian Lower Wuerhe Formations (P_{2w}). Cao et al. (2005, 2006) determined oil sources and documented oil migration and mixing as well as a Permian hybrid petroleum system in the northwest margin of the Junggar Basin based on the tricyclic terpane distribution pattern suggested by Wang and Kang (1999, 2001).

Permian source rock samples studied to date were collected from the border areas of the basin (Zhou et al., 1989; Yang et al., 1992; Zhang et al., 1993). Source rocks of the Lower Permian Jiamuhe (P_{1j}) and Fengcheng (P_{1f}) and Middle Permian Lower Wuerhe (P_{2w}) formations are present throughout the Mahu sag as well as sags in the central Junggar Basin based on seismic data (Jia et al.,

1992; Zhang et al., 1993); however, they have not been drilled in the central area of these sags so far due to their great burial depths. These source rocks vary substantially both in facies and maturities within the basin or even over a sag-wide scale (Zhang et al., 1993). All the molecular parameters which were used for oil source correlation in these previous studies can be influenced by facies and maturity variations (e.g., Peters et al., 2005). Although it is quite certain that oils in the northwestern and central areas of Junggar Basin are derived from Permian strata it remains unclear from which Permian formation the oils in individual oil reservoirs in these areas are mainly derived (Wang et al., 2013).

In previous studies on oil source correlations in the northwestern and central Junggar Basin, biomarker parameters were heavily used while isotopic data, especially the isotopic compositions of individual n-alkanes were rarely reported (Jiang and Fan, 1983; Jiang and Fowler, 1986; Jiang et al., 1988; Zhou et al., 1989; Yang et al., 1992; Zhang et al., 1993; Clayton et al., 1997; Wang and Kang, 1999, 2001; Pan and Yang, 2000; Pan et al., 2003; Cao et al., 2005, 2006; Wang et al., 2008; Xiang et al., 2015). For oil

reservoirs in the northwestern and central areas of the Junggar Basin, oil components can be derived from multiple source rocks from the Fengcheng, Lower Wuerhe and even Jiamuhe formations (Pan and Yang, 2000; Pan et al., 2003; Cao et al., 2005, 2006; Xiang et al., 2015). The concentrations of biomarkers in the oils (terpanes and steranes) may vary by several orders of magnitude and generally decrease with maturity. Also, the origin of these biomarkers may be different from that of the majority of the oil components. Compound specific isotopic analysis has been well established for nearly 30 years (e.g., Hayes et al., 1987, 1990; Freeman et al., 1990; Bjorøy et al., 1991, 1992, 1994; Clayton, 1991; Clayton and Bjorøy, 1994; Collister et al., 1992, 1994; Eglinton, 1994; Ruble et al., 1994; Schoell et al., 1994; Wilhelms et al., 1994; Xiong and Geng, 2000; Odden et al., 2002; Jia et al., 2010, 2013; Yu et al., 2012, 2014) and is a valuable method in oil-oil and oil-source rock correlation (Peters et al., 2005). For non-biodegraded or slightly biodegraded oils, *n*-alkanes are the major components, in contrast to the biomarkers (e.g., Peters et al., 2005). Therefore, the carbon isotopic compositions (δ^{13}C values) of individual *n*-alkanes and their variation with carbon number are very useful in oil source correlations, especially when these data vary substantially among different source rocks in a basin.

In the present study, we extend the oil source correlation in the northwestern and central areas of the Junggar Basin based on molecular parameters and carbon isotopic compositions of individual *n*-alkanes for oils and extracts of oil-prone source rocks. Previous studies have demonstrated that δ^{13}C values of individual *n*-alkanes become increasingly enriched with maturity (Clayton, 1991; Clayton and Bjorøy, 1994; Collister et al., 1994; Love et al., 1998). In the present study, oils collected from the Mahu sag generally have high maturities. Pyrolysis experiments were performed on kerogens of two Permian source rocks in a confined system (Au capsules) to reveal any maturity effect on *n*-alkane δ^{13}C values and any trend with *n*-alkane carbon number.

2. Geological setting

The Junggar Basin is situated in the north of Xinjiang Uyghur Autonomous Region of China, covering an area of about 130×10^3 km^2 (Fig. 1). It is a composite stacked basin of the central landmass type, characteristic of the Precambrian crystalline and the lower Paleozoic bi-layer basement (Zhao, 1992a,1992b). After the basement of the pre-Carboniferous was shaped, the evolutionary history of the Junggar Basin can be divided into four stages in general: (1) Late Carboniferous to Early Permian: foreland marine–residual marine basin; (2) Middle to Late Permian: interior foreland basin; (3) Triassic to Eogene: intra-craton down-warped basin; and (4) Neogene to Quaternary: reactivated collisional foreland basin (Graham et al., 1990; Song, 1995; Chen et al., 2003).

The generalized stratigraphy in the studied area is shown in Fig. 2. The Middle-Upper Carboniferous is composed mainly of volcanic and clastic sequences. The Permian strata consist mainly of clastic rocks with some volcanic rocks in the lower part. The Triassic and Jurassic strata contain mainly sandstones, mudstones, carbonaceous mudstones and coals deposited in fluvial and shallow lacustrine environments while the Cretaceous, Tertiary and Quaternary strata contain mainly alluvial and fluvial clastic sediments. Source rocks are within the Lower Permian Jiamuhe (P_{1j}), Lower Permian Fengcheng (P_{1f}) and Middle Permian Lower Wuerhe (P_{2w}) formations while the reservoir rocks are present in nearly all formations from the Carboniferous to the Cretaceous (Zhang et al., 1993; Fig. 2).

The Lower Permian Jiamuhe Formation was deposited in a period of intense volcanic eruption and consists of mottled conglomerates, mudstones, volcanic tuff and breccia. This formation is mainly distributed in the northwestern area of the basin (Cao et al., 2005). Source rocks are mainly within the lower part of this formation, such as lacustrine dark gray mudstones and tuffaceous mudstones with TOC up to 2.0%, containing mainly Type III kerogen (Cao et al., 2005). Previous studies have suggested that the source rocks of this formation are gas-prone and the major contributor of gas components in gas reservoirs in the northwestern area of the Junggar Basin (Li et al., 2007; Gao et al., 2012; Liu et al., 2013, 2014). Gas components derived from this formation are characterized by high dryness ratios ($C_1/\Sigma C_{1-4}$) and less negative carbon isotope ratios (Li et al., 2007; Gao et al., 2012; Liu et al., 2013, 2014).

The Lower Permian Fengcheng Formation (P_{1f}) was deposited in saline to hypersaline lagoonal environments, and mainly consists of dark dolomitic mudstone, tuffaceous dolomite, and tuffaceous dolomitic mudstone. Source rocks within this formation, collected from boreholes in the northwestern border area of the basin, mainly contain Type I kerogen, with TOC contents ranging from 1.26 to 4.92% (Jiang and Fan, 1983). The Fengcheng Formation has a wider distribution than the Jiamuhe Formation. The source rocks of the Fengcheng Formation are thickest in the northern area of the Mahu sag, and become thinner southward (Zhang et al., 1993; Cao et al., 2005). Previous studies generally concluded that source rocks of the Fengcheng Formation are the most important contributor of oil components in oil reservoirs in the northwestern area of the Junggar Basin (Zhou et al., 1989; Yang et al., 1992; Zhang et al., 1993; Cao et al., 2005).

The Middle Permian Lower Wuerhe Formation (P_{2w}) was deposited in fluvial, alluvial-swamp and lacustrine facies, and contains conglomerates, muddy sandstones and mudstones. This formation mainly consists of coarse clastic sediments with minor mudstones containing gas-prone kerogen in the northwestern border area of the basin (Zhang et al., 1993). Ten mudstone cores collected from the Lower Wuerhe Formation in the burial interval 3888–5247 m in borehole AC1 (Fig. 1) contain only gas-prone kerogen (Yang et al., 1985). However, it has been suggested that this formation was deposited in a semi-deep to deep lacustrine facies in the central Mahu sag and in the central area of the basin, and mainly consists of dark mudstones and shales rich in organic matter dominated by oil-prone kerogen (Zhang et al., 1993). In addition, Permian oil-prone source rocks have been identified within the Pingdiquan Formation (P_{2p}) in the eastern area and the Lucaogou Formation (P_{2l}) in the southern area of the basin (e.g., Zhou et al., 1989; Graham et al., 1990; Carrol et al., 1992; Yang et al., 1992; Zhang et al., 1993; King et al., 1994; Clayton et al., 1997; Carroll, 1998). Both formations are age-equivalent analogs of the Lower Wuerhe Formation (P_{2w}) in the northwestern area based on fossil data (Fig. 3; Zhang et al., 1993; P. Li et al., 2010; S. Li et al., 2010). Fortunately, a column of dark mudstone core was obtained from the Lower Wuerhe Formation at a depth of around 4660 m from borehole JT1 drilled in 2013 in the Zhongguai uplift, southwest of the Mahu sag (Fig. 1). This core was only 0.50 m in length and was designed for the analysis on petrophysical data of caprocks. It consists of oil-prone source rocks with TOC and Rock–Eval hydrogen indices (HI) up to 3.37% and 550 mg/g TOC, respectively (Table 1). Analytical data from this core confirms that the Lower Wuerhe Formation consists of oil-prone source rocks in this region.

3. Samples and experimental

3.1. Samples

Twelve source rocks and 78 oils were collected in the present study (Tables 1 and 2, Fig. 1). For the 12 source rocks, nine samples were collected within the Lower Permian Fengcheng Formation

Erathem	System	Series	Formation	Lithology	Thickness (m)	Combinations
Cenozoic	Quaternary				0-880	
	Tertiary					
Mesozoic	Cretaceous	Lower	Tugulu(K_1tg)		130-1491	
	Jurassic	Upper	Qigu(J_3q)		0-120	
		Middle	Toutunhe(J_2t)		0-210	
			Xishanyao(J_2x)		15-268	
		Lower	Sangonghe(J_1s)		0-425	
			Badaowan(J_1b)		0-729	
	Triassic	Upper	Baijiantan(T_3b)		40-415	
		Middle	Karamay(T_2k)		30-506	
		Lower	Baikouquan(T_1b)		130-436	
Paleozoic	Permian	Upper	Upper Wuerhe(P_3w)		10-920	
		Middle	Lower Wuerhe(P_2w)		830-1850	
			Xiazijie(P_2x)		850-1160	
		Lower	Fengcheng(P_1f)		430-1170	
			Jiamuhe(P_1j)		400-1800	
	Carboniferous					

Legend: Mudstone, Silty mudstone, Muddy sandstone, Sandstone, Sandy conglomerate, Conglomeratic siltstone, Muddy limestone, Muddy dolomite, Tuffaceous dolomite, Tuff, Andesite, Basalt, Coal seam, Source rock, Reservoir rock, Ultimate cap rock, Primary cap rock

Fig. 2. Stratigraphy of the northwestern and central Junggar Basin (modified from Cao et al., 2005).

(P_{1f}) from five boreholes at the northern border of the Mahu sag. One sample was collected within the Middle Permian Lower Wuerhe Formation from borehole JT1 in the Zhongguai uplift at the southwestern border of the Mahu sag. The other two samples were collected within the Middle Permian Lucaogou Formation from borehole J23 in the southern area and within the Middle Permian Pingdiquan Formation from borehole SS1 in the eastern area of the Junggar Basin (Table 1, Fig. 1). For the 78 oil samples, 76 oils were collected from the northwestern and central areas of the Junggar Basin while the other two were collected from boreholes J25 and SS011 in the southern and eastern areas of the Junggar Basin (Table 2, Fig. 1).

3.2. Total organic carbon content (TOC), Rock-Eval and bitumen extraction of source rocks

All 12 source rocks were first cleaned and then ground into powder (about 200 mesh). A small aliquot of powder was taken from each sample for measurement of TOC using a Leco-230C/S analyzer. Another small aliquot of powder was taken for Rock-

Fig. 3. Permian stratigraphy in different areas of the Junggar Basin.

Table 1
Total organic carbon content (TOC) and Rock-Eval parameters of Permian source rocks.

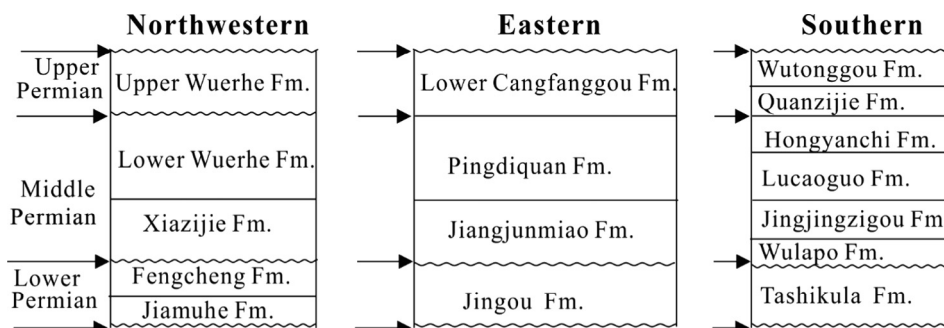|	Depth (m)	Strata	TOC%	HI	T_{max}	1	2	3	4	5	6	7	8	9	10	11	12	13	14
F5S1	3232.7	P_{1f}	1.41	769	428	1.36	1.94	0.91	0.87	0.66	0.26	0.06	0.08	0.06	0.47	0.72	0.02	0.37	0.29
F5S2	3288.6	P_{1f}	1.13	1115	435	1.16	1.97	0.92	1.00	0.80	0.22	0.06	0.09	0.02	0.45	0.64	0.02	0.35	0.30
F5S3	3474.9	P_{1f}	3.01	741	430	2.78	3.23	1.27	0.94	0.70	0.31	0.08	0.07	0.03	0.74	0.73	0.02	0.34	0.21
FN1S1	4096.4	P_{1f}	1.82	505	440	0.83	0.83	1.13	0.50	1.00	0.23	0.46	0.30	0.09	0.19	0.43	0.06	0.46	0.55
FN1S2	4123.8	P_{1f}	1.22	447	437	1.10	1.42	1.06	0.71	1.22	0.26	0.18	0.10	0.04	0.24	0.16	0.05	0.45	0.39
FN4S1	4228.8	P_{1f}	1.95	505	447	1.15	1.33	0.93	0.71	0.80	0.24	0.42	0.16	0.06	0.16	0.42	0.05	0.50	0.56
FN5S1	4065.6	P_{1f}	1.07	290	432	1.47	2.60	0.73	1.71	0.72	0.20	0.07	0.04	0.02	0.19	0.47	0.04	0.50	0.53
X76S1	3455.5	P_{1f}	2.77	523	438	1.23	2.07	0.67	0.61	0.74	0.15	0.20	0.09	0.01	0.16	0.49	0.04	0.41	0.31
X76S2	3455.8	P_{1f}	1.92	524	440	1.29	2.21	0.68	0.67	0.78	0.13	0.21	0.10	0.01	0.16	0.66	0.03	0.38	0.32
JT1S1	4660.6	P_{2w}	3.37	550	450	0.51	0.37	1.61	0.58	1.11	0.16	0.69	0.39	0.13	0.12	0.35	0.25	0.46	0.55
J23S3	2295.9	P_{2l}	7.76	663	444	1.59	2.26	0.89	0.98	1.16	0.03	0.23	0.16	0.01	0.14	0.21	0.02	0.16	0.24
SS1S3	2276.4	P_{2p}	5.01	698	449	0.58	0.27	2.08	0.61	1.02	0.10	0.46	0.31	0.07	0.07	0.11	0.14	0.37	0.36

HI: in mg/g TOC; T_{max} is in °C; 1: Pr/n-C_{17}; 2: Ph/n-C_{18}; 3: Pr/Ph; 4: C_{20}/C_{21} tricyclic terpanes; 5: C_{21}/C_{23} tricyclic terpanes; 6: tricyclic terpanes/(tricyclic terpanes + C_{30} hopane) = $(C_{20} + C_{21} + C_{23}$ tricyclic terpanes)/3)/(($C_{20} + C_{21} + C_{23}$ tricyclic terpanes)/3 + C_{30} hopane); 7: Ts/(Tm + Ts); 8: C_{29}Ts/(C_{29} hopane + C_{29}Ts); 9: C_{30} diahopane/(C_{30} diahopane + C_{30} hopane);10: gammacerane/(C_{30} hopane + gammacerane); 11: β-carotene/(β-carotene + C_{30} hopane); 12: $C_{21}/(C_{21} + \Sigma C_{29})$ steranes; 13: C_{29} 20S/(20S + 20R) steranes; 14: C_{29} αββ/(ααα + αββ) steranes.

Eval analysis using an IFP Rock-Eval 6. The remaining powdered samples (about 80 g each) were Soxhlet extracted with CH_2Cl_2: CH_3OH, 93:7, v:v) for 72 h to obtain extractable hydrocarbons.

3.3. Oil and bitumen fractionation

The 78 oil samples were deasphaltened using a 40× excess of hexane. The extracted bitumen from the source rocks were first diluted with about 1 ml or less of CH_2Cl_2 and were then deasphaltened using a 40× excess of hexane. All the deasphaltened samples were fractionated on a silica:alumina column using hexane, hexane:CH_2Cl_2 (2:1, v:v) and methanol as eluants to yield the saturated, aromatic and resin fractions, respectively.

3.4. GC, GC–MS and GC–IRMS analyses

Saturated fractions from the crude oils and extracts of source rocks were first analyzed by gas chromatography (GC) using a HP6890 GC fitted with a 30 m × 0.32 mm i.d. HP-5 column with a film thickness of 0.25 μm and using nitrogen as carrier gas. A constant flow mode and a flame ionization detector were employed. The GC oven temperature was held initially at 70 °C for 5 min, ramped from 70 to 295 °C at 4 °C/min, and then held at 295 °C for 30 min.

After GC analysis, the saturated fractions were further treated with urea adduction to separate n-alkanes and iso- and cyclic-alkanes. Gas chromatographic–mass spectrometric analysis of iso- and cyclic-alkane fractions were carried out using a Thermal Scientific DSQ II quadrupole mass spectrometer interfaced to a Trace GC Ultra. The GC Ultra was fitted with a 30 m × 0.25 mm i.d. HP-5MS column with a film thickness of 0.25 μm and using

helium as carrier gas. A constant flow was used. The mass spectrometer was operated in electron impact (EI) mode at 70 eV. The GC oven temperature was initially held at 80 °C for 2 min, ramped from 80 to 180 °C at 8 °C/min, from 180 to 290 °C at 2 °C/min, and then held at 290 °C for 20 min.

Gas chromatography–isotope ratio mass spectrometry (GC–IRMS) analysis on n-alkane fractions was performed on a GV Isoprime IRMS instrument interfaced to a HP6890 GC via a combustion interface. The GC was fitted with a 30 m × 0.25 mm i.d. HP-5MS column with a film thickness of 0.25 μm and using helium as carrier gas. The initial temperature was 80 °C for 1.5 min, ramped from 80 to 130 °C at 20 °C/min, and further from 130 to 290 °C at 4 °C/min, and then held at 290 °C for 15 min. A mixture of n-alkane standards (n-C_{12}, n-C_{14}, n-C_{16}, n-C_{18}, n-C_{20}, n-C_{22}, n-C_{25}, n-C_{28}, n-C_{30}, n-C_{32} and n-C_{35}, provided by A. Schimmelmann of Indiana University, USA) was measured daily to monitor the GC–IRMS system. Replicate analyses of this mixture show that the standard deviation for each compound was < 0.3‰. Carbon isotopic values are reported relative to the VPDB standard. Each sample was analyzed at least twice. The reproducibility was generally within ± 0.4‰. The average for the two or more runs was accepted as the final isotopic result for a sample.

3.5. Pyrolysis in a confined system

Pyrolysis experiments on two kerogens were performed in a confined system (Au capsules) at a fixed pressure of 50 MPa and two heating rates of 2 °C/h or 20 °C/h. The two kerogens were obtained from source rock FN1S1 of the Fengcheng Formation (P_{1f}) and J23S3 of the Lucaogou Formation (P_{2l}, Table 1, Fig. 1). Capsule preparation and details of the pyrolysis method were

Table 2
Molecular parameters for oils.

ON	Oil sample	Strata	Depth (m)	1	2	3	4	5	6	7	8	9	10	11	12	13	14
1	W007O1	T2k	1271–1256	2.03	2.64	0.96	0.95	0.88	0.40	0.14	0.05	0.04	0.29	0.92	0.05	0.47	0.47
2	W42O1	P2w	1213–1258	1.24	1.51	1.06	0.93	0.76	0.38	0.10	0.11	0.04	0.36	0.89	0.04	0.45	0.40
3	FN7O1	P1f	4296–4334	1.07	1.31	1.02	0.88	0.87	0.41	0.10	0.08	0.03	0.30	0.92	0.04	0.47	0.54
4	F21O1	P1f	3368–3385	1.22	1.52	0.99	0.92	0.68	0.37	0.07	0.05	0.03	0.41	0.88	0.04	0.49	0.47
5	FN4O1	P1f	4254–4268	1.22	1.59	0.85	0.87	0.70	0.36	0.13	0.06	0.06	0.33	0.65	0.04	0.48	0.48
6	FN4O2	P1f	4607–4618	1.20	1.49	1.04	0.88	0.73	0.37	0.07	0.06	0.02	0.45	0.88	0.03	0.49	0.52
7	X71O1	P1f	4510–4530	1.00	1.37	0.76	0.47	0.70	0.18	0.59	0.29	0.06	0.28	0.50	0.03	0.44	0.58
8	X72O1	P1f	4808–4826	1.19	1.51	0.90	0.93	0.80	0.74	0.26	0.11	0.05	0.57	0.96	0.08	0.45	0.61
9	X79O1	J1b	1381–1385	1.10	1.22	1.09	0.94	0.83	0.47	0.17	0.12	0.04	0.31	0.49	0.12	0.45	0.54
10	X81O1	T2k2	2155–2187	0.69	0.61	1.32	1.41	1.02	0.59	0.23	0.11	0.07	0.23	0.78	0.19	0.45	0.58
11	X87O1	P1f	4226–4238	0.93	1.14	0.90	0.54	0.90	0.14	0.36	0.16	0.04	0.12	0.29	0.04	0.44	0.55
12	X89O1	T1b2	2452–2474	1.09	1.34	1.05	1.02	0.81	0.56	0.22	0.08	0.06	0.37	0.96	0.07	0.48	0.53
13	X93O1	T1b3	2680–2712	1.10	1.38	0.99	0.97	0.99	0.58	0.16	0.15	0.04	0.30	0.78	0.09	0.45	0.49
14	X94O1	T1b	2914–2923	1.04	1.10	1.19	1.00	0.91	0.58	0.21	0.06	0.06	0.38	0.96	0.08	0.48	0.53
15	X95O1	T1b2	2804–2832	1.02	1.22	1.00	1.07	0.93	0.67	0.25	0.06	0.08	0.28	0.86	0.12	0.49	0.54
16	X01O1	T2K1	1382–1401	1.08	1.14	1.13	1.31	1.04	0.57	0.21	0.08	0.02	0.29	0.63	0.11	0.45	0.51
17	X731-HO1	T1b	3034–3037	1.00	1.17	1.04	0.98	1.01	0.75	0.32	0.02	0.10	0.32	0.94	0.11	0.50	0.56
18	X723O1	T1b	2726–2743	0.92	0.98	1.10	1.07	0.98	0.76	0.36	0.04	0.09	0.35	0.95	0.11	0.47	0.56
19	Ma13O1	T1b	3106–3129	0.95	0.99	1.25	1.21	0.99	0.48	0.28	0.19	0.07	0.29	0.89	0.12	0.43	0.57
20	Ma15O1	T1b	3048–3056	0.94	0.84	1.43	1.44	0.86	0.53	0.15	0.11	0.05	0.38	0.95	0.09	0.46	0.48
20	Ma15O1d	T1b	3048–3056	0.92	0.88	1.31	1.41	1.04	0.67	0.19	0.16	0.05	0.36	0.88	0.13	0.45	0.52
21	Ma19O1	T1b	3522–3588	0.92	0.92	1.20	1.13	0.96	0.65	0.39	0.13	0.06	0.42	0.96	0.16	0.47	0.58
22	Ma005O1	T1b	3367–3379	0.85	0.90	1.14	0.99	0.96	0.78	0.43	0.11	0.13	0.54	0.98	0.22	0.44	0.68
23	Ma131O1	T1b2	3186–3200	0.93	0.92	1.42	1.29	1.10	0.71	0.33	0.06	0.07	0.27	0.98	0.21	0.48	0.58
23	Ma131O1d	T1b2	3186–3200	0.93	0.97	1.18	1.34	1.14	0.79	0.37	0.09	0.07	0.35	0.90	0.28	0.46	0.63
24	Ma134O1	T1b2	3169–3188	0.96	0.99	1.45	0.95	1.11	0.73	0.32	0.08	0.10	0.25	0.98	0.09	0.49	0.56
25	Ma134O2	T1b2	3210–3215	0.96	0.91	1.51	1.21	0.99	0.64	0.17	0.08	0.05	0.31	0.96	0.09	0.48	0.55
25	Ma134O2d	T1b2	3210–3215	0.96	1.01	1.14	1.04	1.10	0.82	0.34	0.16	0.13	0.39	0.91	0.15	0.45	0.62
26	Ma132-HO1	T1b2	3545–4333	0.91	0.97	1.15	1.14	1.06	0.75	0.39	0.13	0.10	0.51	0.97	0.20	0.44	0.63
27	Da1O1	T2k	4244–4252	0.80	0.76	1.21	0.83	0.89	0.79	0.57	0.13	0.14	0.20	0.98	0.25	0.47	0.64
28	Da9O1	T1b	4646–4727	0.85	0.82	1.43	0.93	0.84	0.75	0.65	0.10	0.13	0.31	0.99	0.26	0.48	0.66
29	Da10O1	T1b	4566–4568	0.81	0.93	1.03	0.79	0.93	0.70	0.54	0.10	0.15	0.47	0.97	0.16	0.46	0.65
30	Da11O1	T1b	4292–4303	0.88	0.95	1.12	0.89	1.02	0.88	0.69	0.12	0.16	0.67	0.99	0.26	0.48	0.67
31	YB1O1	P2w	4029–4052	1.07	1.58	1.00	0.91	0.85	0.54	0.31	0.08	0.07	0.25	0.99	0.08	0.49	0.59
32	YB2O1	T1b	4106–4120	0.97	1.14	1.00	0.83	0.90	0.91	0.68	0.11	0.17	0.66	0.99	0.22	0.49	0.68
33	XY2O1	T1b	4325–4407	0.93	1.07	1.07	0.84	0.82	0.64	0.48	0.12	0.12	0.34	0.98	0.12	0.45	0.60
34	Ma202O1	T1b	3789–3802	1.00	1.15	1.01	0.97	0.96	0.90	0.69	0.16	0.15	0.48	0.96	0.30	0.49	0.64
35	Ma18O1	T1b1	3892–3920	0.97	0.94	1.42	1.20	0.99	0.70	0.41	0.10	0.07	0.36	0.99	0.17	0.48	0.63
35	Ma18O1d	T1b1	3892–3920	0.91	0.95	1.16	1.19	1.04	0.69	0.42	0.14	0.04	0.40	0.94	0.18	0.45	0.69
36	MX1O1	T1b	3582–3588	0.94	0.93	1.30	1.20	1.07	0.70	0.31	0.07	0.07	0.38	0.97	0.20	0.49	0.62
37	MZ1O1	T1b	4346–4366	0.87	1.02	0.99	0.84	0.88	0.75	0.55	0.05	0.12	0.41	0.95	0.15	0.47	0.71
38	AH1O1	T1b	3848–3862	0.86	0.88	1.14	1.08	1.10	0.71	0.48	0.17	0.09	0.50	0.96	0.21	0.47	0.66
39	AH2O1	T1b2	3310–3336	0.88	0.95	1.08	1.05	1.04	0.60	0.44	0.13	0.09	0.45	0.95	0.19	0.45	0.60
40	AH5O1	T1b3	3796–3800	0.77	0.73	1.22	1.51	1.14	0.74	0.28	0.17	0.05	0.42	0.97	0.25	0.48	0.62
41	AH6O1	T1b2	3878–3909	0.89	0.90	1.18	1.16	1.10	0.79	0.52	0.02	0.05	0.40	0.97	0.26	0.51	0.67
42	AH012O1	T1b2	3839–3864	0.90	0.95	1.08	1.04	1.02	0.64	0.35	0.14	0.10	0.46	0.50	0.15	0.49	0.57
43	AH013O1	T1b	3798–3816	0.89	0.95	1.13	1.10	1.00	0.75	0.43	0.02	0.08	0.44	0.96	0.23	0.53	0.67
44	Ke92O1	C	576–588	0.97	1.11	1.13	0.98	1.02	0.50	0.10	0.04	0.03	0.30	0.95	0.10	0.47	0.52
45	Ke94O1	C	1324–1350	1.14	1.41	1.25	1.00	1.00	0.51	0.15	0.04	0.05	0.28	0.95	0.10	0.48	0.53
46	Ke301O1	P1j	3863–3866	0.61	0.60	1.47	0.93	1.22	0.72	0.37	0.16	0.07	0.28	0.65	0.21	0.47	0.50
47	Ke302O1	P3w	3642–3670	0.77	0.79	1.42	0.81	1.05	0.57	0.24	0.06	0.09	0.26	0.96	0.11	0.46	0.54
48	Ke901O1	C	1152–1172	0.43	0.36	1.62	0.86	1.16	0.28	0.26	0.12	0.06	0.10	0.77	0.11	0.49	0.54
49	G25O1	J1s	2971–2979	0.33	0.19	2.26	0.75	1.12	0.29	0.36	0.13	0.11	0.21	0.72	0.10	0.48	0.56
50	G28O1	J1s	2901–2916	0.35	0.25	1.70	0.77	0.88	0.36	0.26	0.10	0.11	0.25	0.78	0.12	0.50	0.55
51	G28O2	J1s	2934–2945	0.33	0.25	1.69	0.72	0.90	0.36	0.28	0.13	0.11	0.27	0.67	0.12	0.50	0.52
52	MH1O1	T1b	3286–3316	0.69	0.73	1.40	0.96	1.33	0.60	0.17	0.11	0.04	0.23	0.93	0.11	0.48	0.54
53	JL1O1	T1b	2704–2709	0.64	0.62	1.23	0.93	1.09	0.64	0.28	0.10	0.08	0.25	0.90	0.11	0.50	0.55
54	JT1O1	P1j	4696–4704	0.44	0.39	1.33	0.82	1.16	0.75	0.70	0.49	0.26	0.28	0.88	0.24	0.48	0.62
55	HS4O1	T2k	1873–1876	1.39	1.18	1.30	0.81	1.06	0.46	0.36	0.11	0.06	0.27	0.94	0.12	0.47	0.49
56	HS5O1	C	1975–1985	0.52	0.49	1.28	0.74	1.03	0.37	0.25	0.11	0.06	0.23	0.63	0.09	0.43	0.49
57	HS6O1	J3q	800–803	1.32	0.63	1.36	0.84	1.02	0.47	0.28	0.11	0.06	0.24	0.02	0.61		
58	HS6O2	C	1046–1086	0.69	0.66	1.11	0.75	1.02	0.54	0.29	0.08	0.04	0.23	0.92	0.12	0.50	0.57
59	H94O1	C	1874–1892	0.85	1.02	1.07	0.84	1.06	0.28	0.12	0.05	0.03	0.20	0.58	0.06	0.43	0.44
60	H022O1	C	2766–2769	0.49	0.46	1.25	0.85	1.03	0.47	0.43	0.21	0.10	0.25	0.72	0.12	0.45	0.53
61	H015O1	T2k1	1966–1971	6.30	2.73	1.26	0.75	1.10	0.48	0.22	0.18	0.05	0.23	0.69	0.12	0.45	0.48
62	G26O1	T2k1	2652–2655	0.44	0.42	1.31	0.83	1.10	0.41	0.16	0.05	0.04	0.28	0.93	0.13	0.46	0.45
63	C43O1	P1j	2155–2170	0.45	0.46	1.05	0.75	1.01	0.72	0.46	0.08	0.12	0.39	0.90	0.12	0.46	0.58
64	CP2O1	K1tg	2026–2032	0.54	0.45	1.54	0.82	1.33	0.26	0.30	0.16	0.05	0.16	0.19	0.13	0.42	0.54
65	CP3O1	P1j	3620–3627	0.43	0.48	0.97	0.73	0.97	0.59	0.36	0.18	0.09	0.36	0.83	0.09	0.44	0.52
66	XG1O1	P1j	4552–4566	0.45	0.46	1.24	0.79	1.17	0.89	0.62	0.47	0.18	0.60	0.98	0.29	0.47	0.59
67	CF5O1	C	1750–1756	2.24	1.88	0.48	0.80	1.25	0.37	0.32	0.15	0.07	0.20	0.12	0.13	0.45	0.53
68	QS1O1	J1s	3943–3946	0.41	0.28	2.06	0.89	1.19	0.67	0.31	0.11	0.07	0.18	0.71	0.28	0.49	0.55
69	Pen5O1	K1tg		0.47	0.33	1.89	0.96	1.33	0.70	0.29	0.21	0.10	0.18	0.56	0.40	0.42	0.53
70	MB11O1	J1	3707–3714	0.45	0.36	1.57	0.81	1.16	0.29	0.22	0.09	0.05	0.10	0.78	0.10	0.49	0.54

Table 2 (continued)

ON	Oil sample	Strata	Depth (m)	1	2	3	4	5	6	7	8	9	10	11	12	13	14
71	Mo7O1	J1s	4239–4262	0.51	0.43	1.73	0.80	1.16	0.32	0.24	0.10	0.06	0.10	0.77	0.12	0.48	0.55
72	Mo21O1	J1s	4351–4363	0.47	0.38	1.76	0.76	1.17	0.46	0.25	0.10	0.08	0.23	0.75	0.17	0.50	0.55
73	Mo22O1	J1s	4598–4618	0.55	0.45	1.59	0.84	1.24	0.24	0.21	0.10	0.07	0.16	0.76	0.07	0.47	0.52
74	XY11O1	J1s	2383–2389	0.35	0.26	1.50	0.82	0.97	0.37	0.29	0.21	0.13	0.22	0.77	0.16	0.46	0.57
75	XY13O1	J1s	2292–2294	0.36	0.26	1.47	0.88	1.13	0.32	0.30	0.20	0.12	0.24	0.81	0.12	0.46	0.57
76	MD4O1	J1s	2261–2266	0.37	0.29	1.41	0.82	1.05	0.35	0.30	0.18	0.12	0.22	0.74	0.13	0.47	0.55
77	J25O1	P2l	3403–3425	1.51	1.36	1.22	0.69	0.98	0.04	0.05	0.14	0.01	0.12	0.34	0.03	0.46	0.27
78	SS011O1	P2p	2374–2379	0.84	0.72	1.28	0.99	1.36	0.14	0.13	0.07	0.02	0.13	0.32	0.06	0.45	0.32

ON: oil number; Suffix "d": duplicates; 1: Pr/n-C$_{17}$; 2: Ph/n-C$_{18}$; 3: Pr/Ph; 4: C$_{20}$/C$_{21}$ tricyclic terpanes; 5: C$_{21}$/C$_{23}$ tricyclic terpanes; 6: tricyclic terpanes/(tricyclic terpanes + C$_{30}$ hopane) = (C$_{20}$ + C$_{21}$ + C$_{23}$ tricyclic terpanes)/3)/((C$_{20}$ + C$_{21}$ + C$_{23}$ tricyclic terpanes)/3 + C$_{30}$ hopane); 7: Ts/(Tm + Ts); 8: C$_{29}$Ts/(C$_{29}$ hopane + C$_{29}$Ts); 9: C$_{30}$ diahopane/(C$_{30}$ diahopane + C$_{30}$ hopane); 10: gammacerane/(C$_{30}$ hopane + gammacerane); 11: β-carotane/(β-carotane + C$_{30}$ hopane); 12: C$_{21}$/(C$_{21}$ + ΣC$_{29}$) steranes; 13: C$_{29}$ 20S/(20S + 20R) steranes; 14: C$_{29}$ αββ/(ααα + αββ) steranes; The amounts of terpanes were measured on m/z 191 mass chromatograms, steranes were measured on m/z 217 mass chromatograms, and carotanes were measured on m/z 125 mass chromatograms.

described previously (Xiang et al., 2016). Oil pyrolysates were recovered for carbon isotope analysis of individual n-alkanes from capsules which were heated to 333.3, 345.5, 418.8 and 430.7 °C at 20 °C/h and 334.9, 346.8, 382.9 and 395.1 °C at 2 °C/h. n-Alkane separation and GC–IRMS analytic conditions for the oil pyrolysates were the same as for oil samples and extracts of source rocks

4. Results

TOC and Rock-Eval hydrogen index (HI) and T_{max} values for the 12 source rocks were 1.07–7.76%, 290–1115 mg/g TOC and 428–450 °C, respectively (Table 1). The selected molecular parameters for 12 source rocks and 78 oils are shown in Tables 1 and 2 and Fig. 4. The gas chromatograms and m/z 191 and m/z 217 mass chromatograms for six source rocks and eight oils are shown in Figs. 5–9. The carbon isotopic compositions of individual n-alkanes for 12 source rocks, pyrolysates of two kerogens and 78 oils are shown in Fig. 10.

5. Discussion

5.1. Differences among Permian source rocks

5.1.1. Molecular geochemistry

For the three source rocks of Middle Permian age, two source rocks JT1S1 and SS1S3 from the Lower Wuerhe Formation (P$_{2w}$) in the northwestern area and Pingdiquan Formation (P$_{2p}$) in the eastern area, respectively have lower Pr/n-C$_{17}$ and Ph/n-C$_{18}$ ratios and higher Pr/Ph ratios, compared with the nine source rocks from the Fengcheng Formation of Early Permian age (P$_{1f}$). In contrast, J23S3 from the Lucaogou Formation (P$_{2l}$) in the southern area has similar values to the nine source rocks of the Fengcheng Formation (P$_{1f}$, Table 1, Figs. 4a, 5, and 6).

Source rocks JT1S1, J23S3 and SS1S3 have a lower relative concentration of gammacerane than the nine source rocks of Lower Permian Fengcheng Formation (Figs. 4b, 5, and 6). However, the relative concentration of gammacerane varies substantially among the nine source rocks of the Fengcheng Formation. For some source rocks, it is spectacularly high (Fig. 5b). For some others, it is much lower and close to that of the three source rocks of Middle Permian age (Figs. 5e, h and 6).

Source rocks JT1S1, J23S3 and SS1S3 generally have lower β-carotane/(β-carotane + C$_{30}$ hopane) ratios than the source rocks of the Fengcheng Formation: 0.11–0.35 for the former and 0.16–0.73 for the latter (Table 1, Fig. 4b). Ts/(Tm + Ts), C$_{29}$Ts/(C$_{29}$ hopane + C$_{29}$Ts) and C$_{30}$ diahopane/(C$_{30}$ diahopane + C$_{30}$ hopane) ratios for source rock JT1S1 are 0.69, 0.39 and 0.13, respectively, substantially higher than those of the other 11 source rocks. These three ratios for source rocks J23S3 and SS1S3 are in the range of those

for the nine source rocks of the Fengcheng Formation (Table 1 and Fig. 4c). For source rocks of the Fengcheng Formation, the amounts of Ts, C$_{29}$Ts and C$_{30}$ diahopane also vary substantially. For some source rocks, they were nearly undetectable (Fig. 5b). For some others, they are particularly high, similar to those of source rocks of Middle Permian age (Figs. 5e, h and 6).

Source rocks JT1S1, J23S3 and SS1S3 show similar patterns of tricyclic terpanes with C$_{20}$ < C$_{21}$ and C$_{21}$ > C$_{23}$ (Fig. 4d). For the nine source rocks of the Fengcheng Formation, five have a distribution pattern of tricyclic terpanes with C$_{20}$ < C$_{21}$ < C$_{23}$ while the other four have C$_{20}$ > C$_{21}$ > C$_{23}$, C$_{20}$ = C$_{21}$ < C$_{23}$, C$_{20}$ < C$_{21}$ = C$_{23}$ and C$_{20}$ > C$_{21}$ and C$_{21}$ < C$_{23}$, respectively (Fig. 4d).

Ratios of tricyclic terpanes/(tricyclic terpanes + C$_{30}$ hopane) and C$_{21}$/(C$_{21}$ + ΣC$_{29}$) steranes are both facies- and maturity-dependent parameters (e.g., Peters et al., 2005). They were 0.13–0.31 and 0.02–0.06, respectively for the nine source rocks of the Fengcheng Formation. They were 0.16, 0.03 and 0.10, and 0.25, 0.02 and 0.14, respectively for JT1S1, J23S3 and SS1S313 (Table 1, Fig. 4e). C$_{29}$ steranes 20S/(20S + 20R) and αββ/(ααα + αββ) ratios are typical molecular maturity parameters (e.g., Peters et al., 2005). They were 0.34–0.50 and 0.21–0.56, respectively for the nine source rocks of the Fengcheng Formation. They were 0.46, 0.16 and 0.37, and 0.55, 0.24 and 0.36, respectively for JT1S1, J23S3 and SS1S313 (Table 1, Fig. 4f).

The measured %Ro for source rock JT1S1 and F5S3 are 1.18 and 0.96, respectively. Previous studies reported that measured %Ro values fall in the range 0.85–1.05 for source rocks of the Fengcheng Formation within the interval 3100–3500 m in boreholes F1, F5 and F7 (Fig. 1, Zhou et al., 1989). %Ro values for J23S3 and SS1S3 were estimated to be 0.5–0.6 (Xiang et al., 2016).

5.1.2. Carbon isotopic compositions of individual n-alkanes for extracts

For source rocks JT1S1, J23S3 and SS1S3, the δ^{13}C values of individual n-alkanes are lower than −32‰ and have a similar trend which decreases with carbon number to the lowest value at n-C$_{25}$, and then increases with n-alkane carbon number (Fig. 10a). For the nine source rocks of the Fengcheng Formation, the δ^{13}C values of individual n-alkanes are generally higher than −32‰ and generally remain stable with increasing carbon number (Fig. 10a).

It is noteworthy that molecular parameters vary substantially among source rocks JT1S1, J23S3 and SS1S3 of Middle Permian age and among the nine source rocks of the Lower Permian Fengcheng Formation, and overlap significantly between these two source rock groups (Fig. 4a–d). Each group of source rocks has similar δ^{13}C values for the individual n-alkanes and a similar trend of δ^{13}C values with increasing n-alkane carbon number, but differ substantially from the other group of source rocks in these isotopic features. The causes behind this phenomenon remain unknown to us.
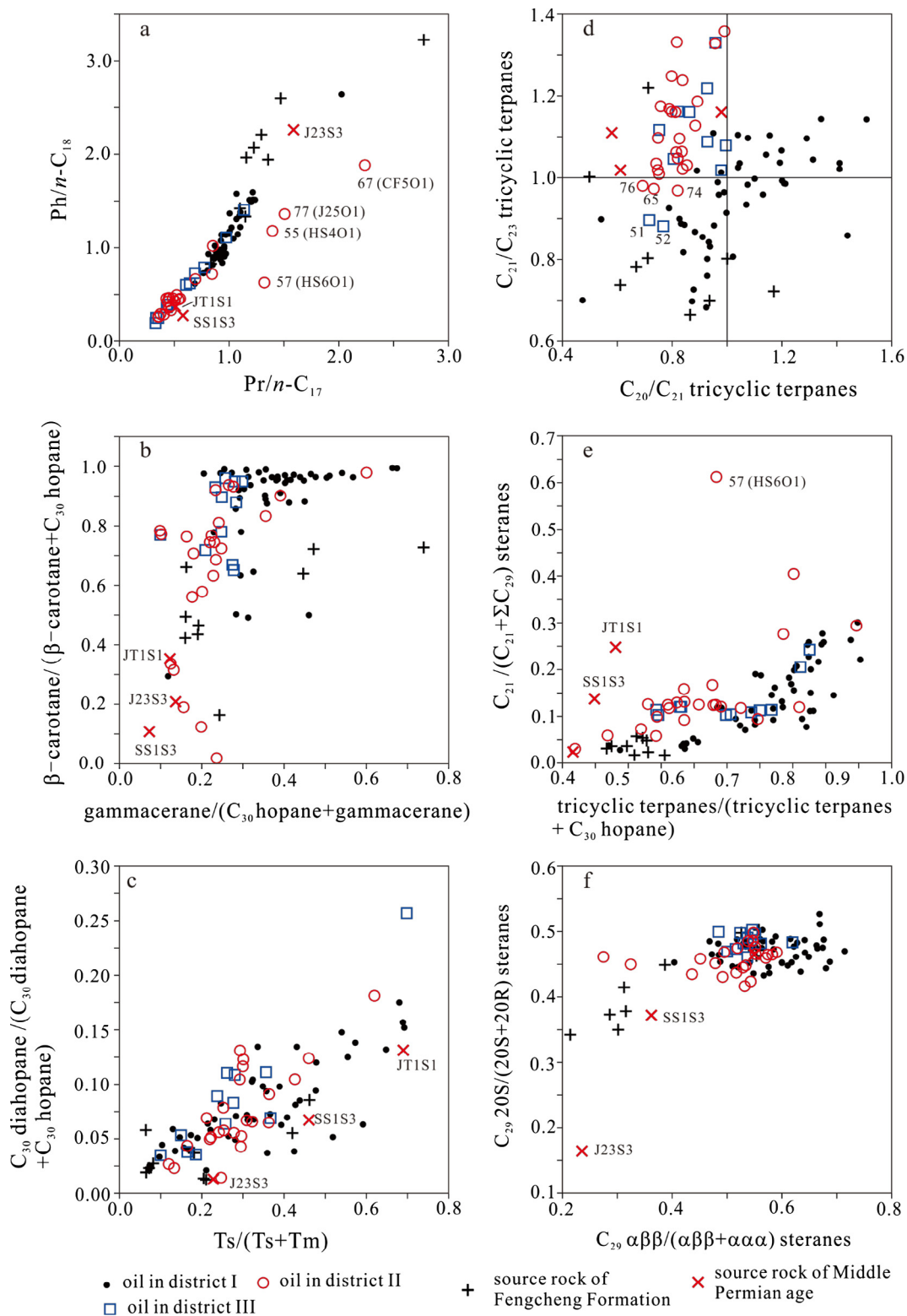
Fig. 4. Crossplots of molecular parameters for oils and extracts from source rocks. (a) crossplot of the ratios of Pr/n-C$_{17}$ vs Ph/n-C$_{18}$; (b) crossplot of the ratios of gammacerane/(C$_{30}$ hopane + gammacerane) vs β-carotane/(β-carotane + C$_{30}$ hopane); (c) crossplot of the ratios of Ts/(Ts + Tm) vs C$_{30}$ diahopane/(C$_{30}$ diahopane + C$_{30}$ hopane); (d) crossplot of the ratios of C$_{20}$/C$_{21}$ tricyclic terpanes vs C$_{21}$/C$_{23}$ tricyclic terpanes; (e) crossplot of the ratios of tricyclic terpanes/(tricyclic terpanes + C$_{30}$ hopane) vs C$_{21}$/(C$_{21}$ + ΣC$_{29}$) steranes; (f) crossplot of the ratios of C$_{29}$ αββ/(ααα + αββ) steranes vs C$_{29}$ 20S/(20S + 20R) steranes.

5.1.3. Carbon isotopic compositions of individual n-alkanes in oil pyrolysates

Previous studies have suggested that δ^{13}C values of individual n-alkanes increase with increasing maturity (Clayton, 1991; Clayton and Bjorøy, 1994; Collister et al., 1994; Love et al., 1998). In the present study, oil pyrolysates from kerogens FN1S1 and J23S3 were analyzed for δ^{13}C values of individual n-alkanes.
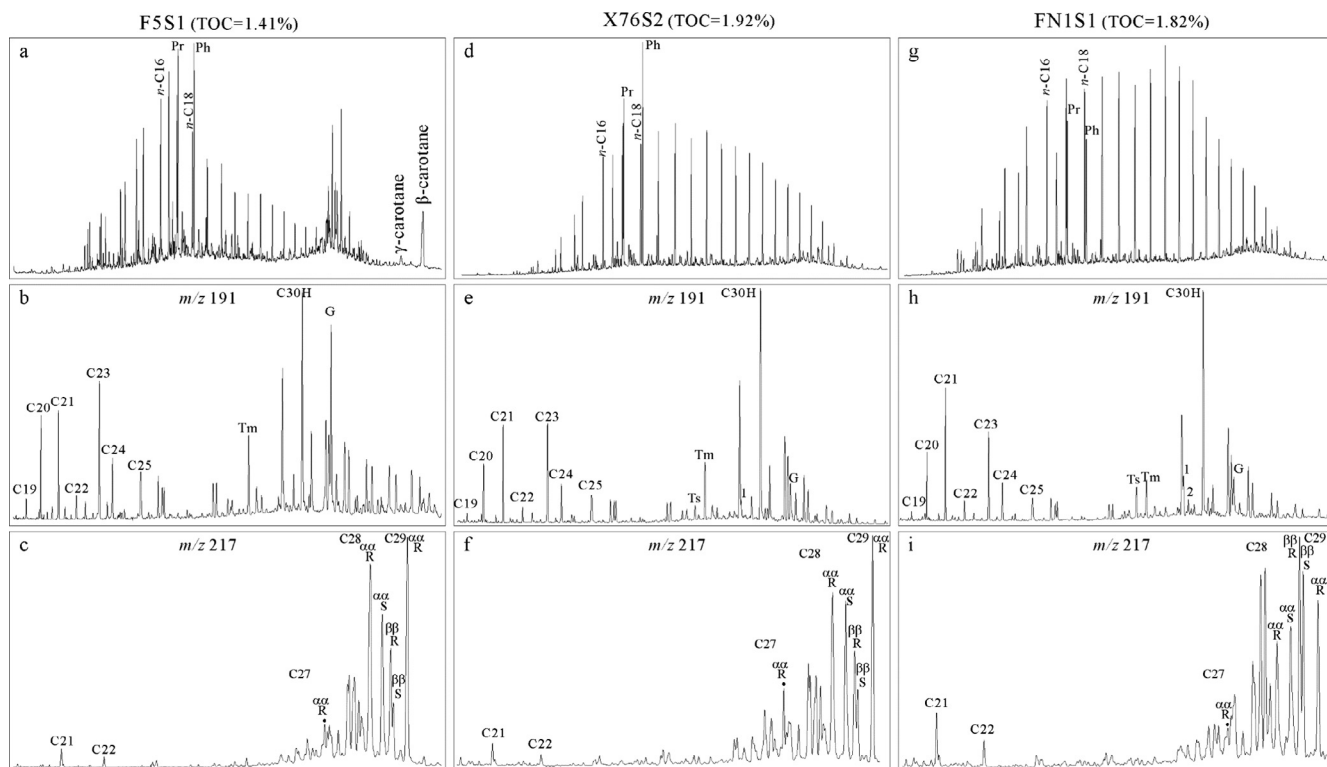
Fig. 5. Gas chromatograms and *m/z* 191 and *m/z* 217 mass chromatograms of extracts from source rocks F5S1, X76S2 and FN1S1 within the Lower Permian Fengcheng Formation (P$_{1f}$). In (b), (e) and (h), C19–C25: C$_{19}$ to C$_{25}$ tricyclic terpanes; 1: C$_{29}$Ts; 2: C$_{30}$ diahopane; G: gammacerane.
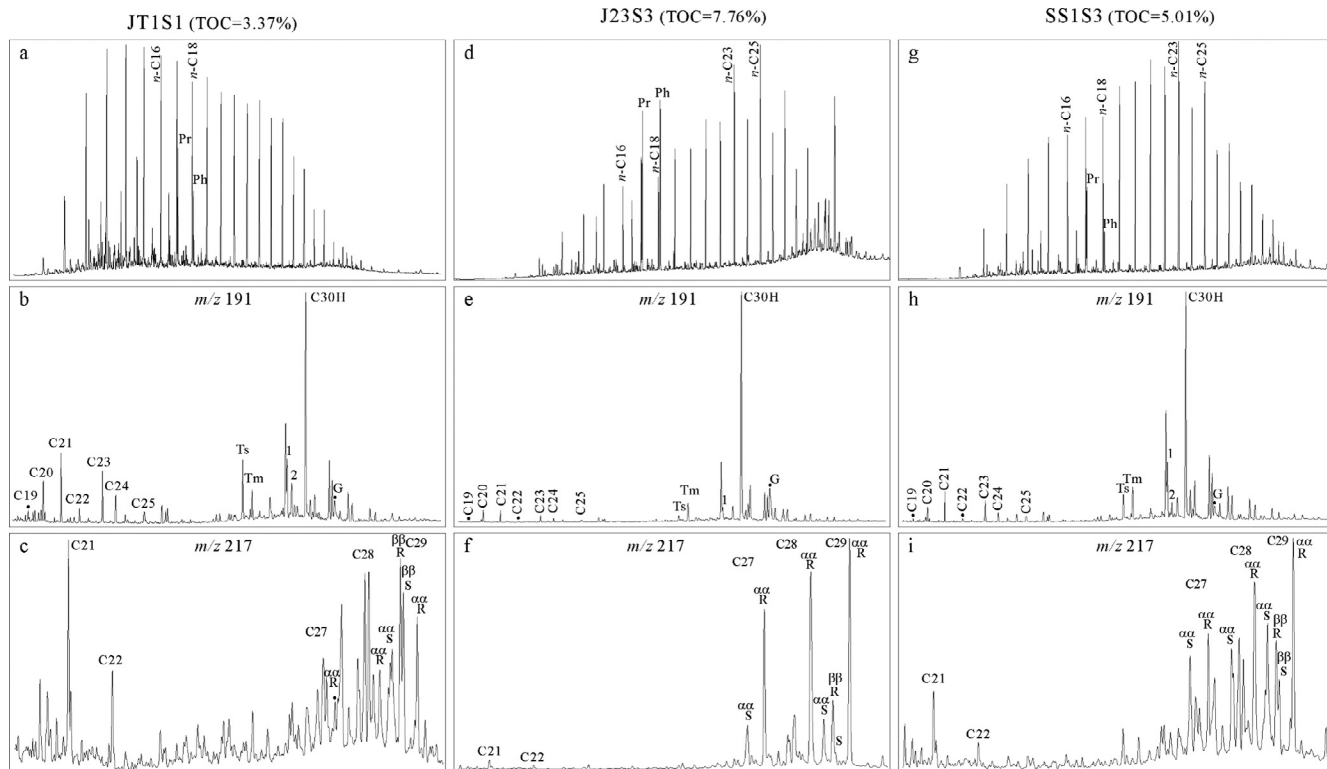
Fig. 6. Gas chromatograms and *m/z* 191 and *m/z* 217 mass chromatograms of extracts from source rocks JT1S1, J23S3 and SS1S3 within the Middle Permian Lower Wuerhe (P$_{2w}$), Lucaogou (P$_{2l}$) and Pingdiquan (P$_{2p}$) formations. In (b), (e) and (h), C19–C25: C$_{19}$ to C$_{25}$ tricyclic terpanes; 1: C$_{29}$Ts; 2: C$_{30}$ diahopane; G: gammacerane.

Sweeney and Burnham (1990) presented a vitrinite maturation model to calculate the vitrinite reflectance (%Ro), called EASY%Ro, using an Arrhenius first-order parallel-reaction approach with a distribution of activation energies. EASY%Ro values were used as a maturity parameter to indicate thermal stress in isothermal or non-isothermal confined pyrolysis experiments (e.g., Hill et al.,
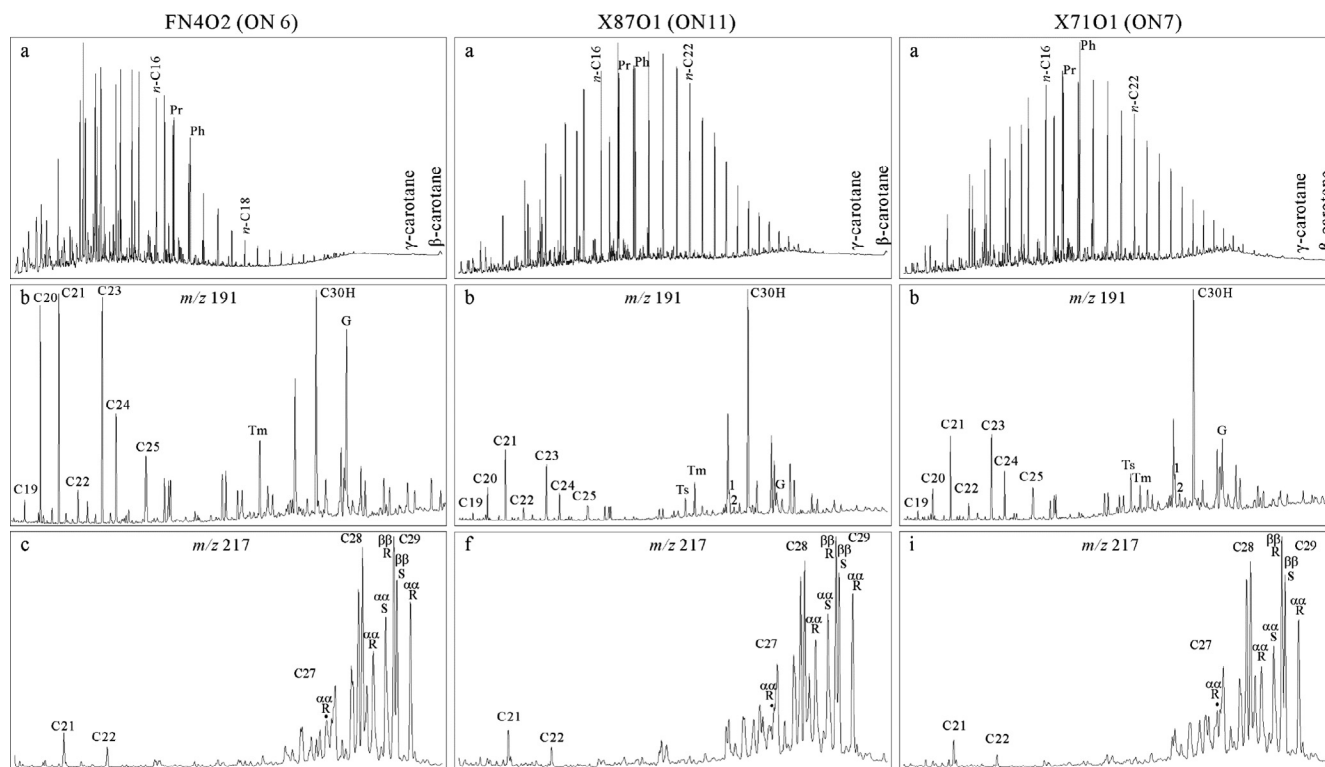
Fig. 7. Gas chromatograms and m/z 191 and m/z 217 mass chromatograms of selected group I oils FN4O2, X87O1 and X71O1. In (b), (e) and (h), C19–C25: C_{19} to C_{25} tricyclic terpanes; 1: C_{29}Ts; 2: C_{30} diahopane; G: gammacerane.
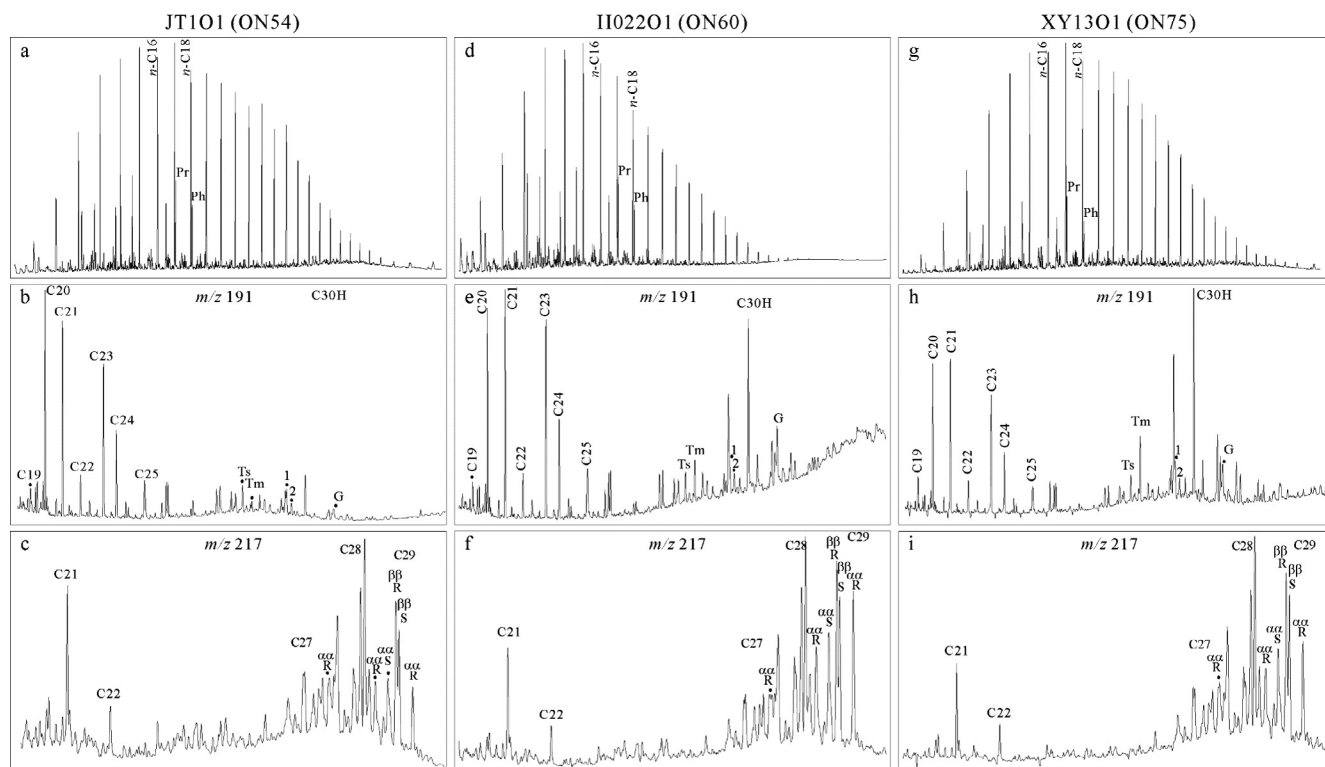
Fig. 8. Gas chromatograms and m/z 191 and m/z 217 mass chromatograms of selected group II oils JT1O1, H022O1 and XY13O1. In (b), (e) and (h), C19–C25: C_{19} to C_{25} tricyclic terpanes; 1: C_{29}Ts; 2: C_{30} diahopane; G: gammacerane.

2003; Li et al., 2013; Xiang et al., 2016). The initial %Ro values for FN1S1 and J23S3 prior to heating were estimated to be about 0.90 and 0.50–0.60, respectively, referenced from previous studies (Zhou et al., 1989; Xiang et al., 2016). EASY%Ro values are 0.90, 0.90, 1.10 and 1.20 for oil pyrolysates of FN1S1, and 0.56, 0.61, 1.05 and 1.18 for oil pyrolysates of J23S3 corresponding to temper-
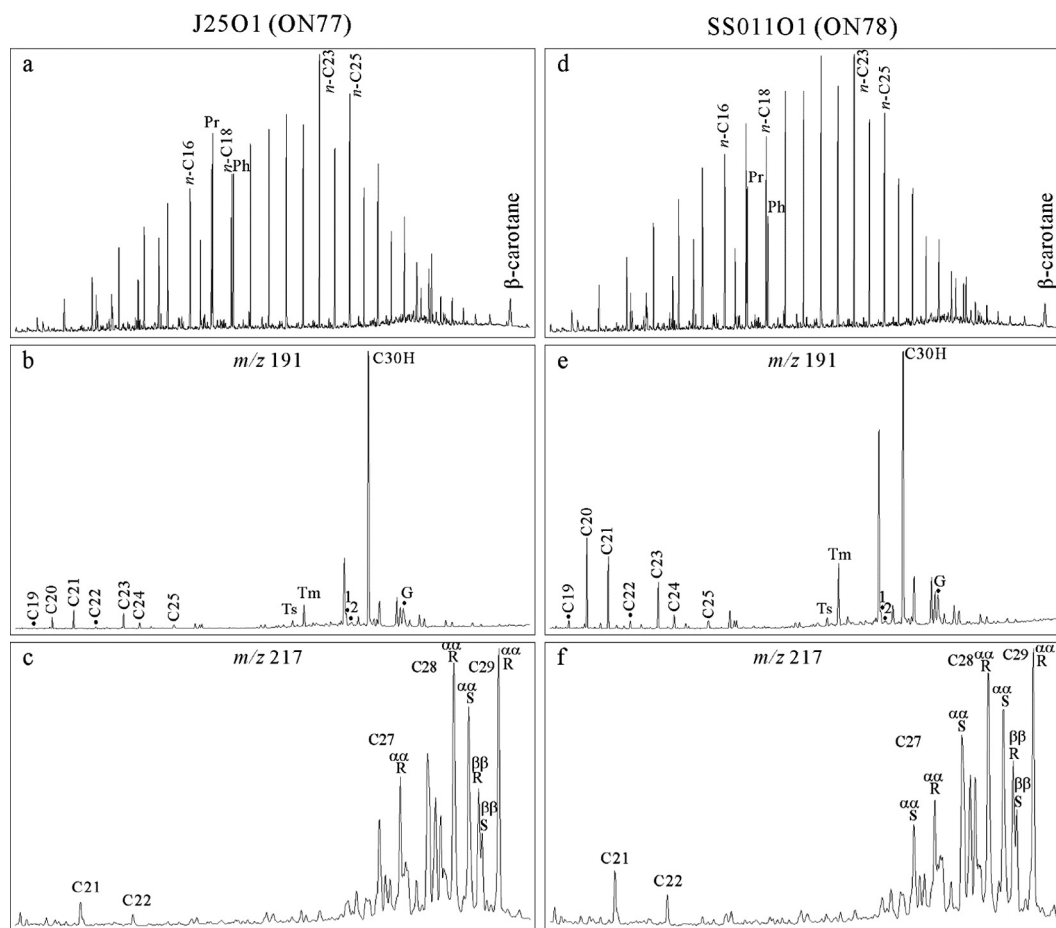
Fig. 9. Gas chromatograms and *m/z* 191 and *m/z* 217 mass chromatograms of oils J25O1 and SS011O1 from the eastern Junggar Basin. In (b) and (e), C19–C25: C$_{19}$ to C$_{25}$ tricyclic terpanes; 1: C$_{29}$Ts; 2: C$_{30}$ diahopane; G: gammacerane.

atures 333.3, 345.5, 418.8 and 430.7 °C, respectively at a heating rate of 20 °C/h. They are 0.92, 0.93, 1.11 and 1.22 for oil pyrolysates of FN1S1, and 0.72, 0.78, 1.07 and 1.21 for oil pyrolysates of J23S3 corresponding to temperatures 334.9, 346.8, 382.9 and 395.1 °C, respectively at heating rate 2 °C/h (Fig. 10b and c).

For FN1S1, the δ^{13}C values of individual *n*-alkanes in the oil pyrolysates are higher than those of the extract, and increase consistently with temperature and EASY%Ro value. The same trends in δ^{13}C values with increasing *n*-alkane carbon number were observed among the extracts and oil pyrolysates at various temperatures and both heating rates (Fig. 10b).

For J23S3, δ^{13}C values of individual *n*-alkanes in the oil pyrolysates are also higher than those of the extract. At 20 °C/h, *n*-alkane δ^{13}C values are very similar, and do not show any increasing trend from 333.3, 345.5 to 418.8 °C, but they increase substantially at 430.7 °C. At 2 °C/h, *n*-alkane δ^{13}C values in the oil pyrolysates increase consistently with temperatures and EASY%Ro value. The trends in δ^{13}C values are generally similar among the extracts and oil pyrolysates at various temperatures and EASY%Ro value. However, the extents of reversal of δ^{13}C values with increasing carbon number in the oil pyrolysates are smaller than the extract, and decrease consistently with temperatures and EASY%Ro (Fig. 10c).

5.2. Oil source correlation

5.2.1. Oil source correlation using carbon isotopic compositions of individual n-alkanes

The 78 oils can be classified into two groups based on δ^{13}C values of individual *n*-alkanes and their variation with carbon num-

ber. For group I oils with oil numbers (ON) from 1–43 (Table 2, Fig. 1), *n*-alkane δ^{13}C values are relatively higher and generally remain stable with increasing carbon number (Fig. 10d). In contrast, for group II oils with ON from 55–76 (Table 2, Fig. 1), δ^{13}C values are relatively lower and decrease at first, and then increase with carbon number (Fig. 10e). Group I oils mainly occur in the central and northern areas of the Mahu sag and surrounding areas, labeled as district I in Fig. 1. Group II oils mainly occur in the southwestern area of the Zhongguai uplift, eastern area of Xiayan uplift, Penyijingxi sag, Mobei uplift and Mosouwan uplift, labeled as district II in Fig. 1. For oils with ON from 44–54 (Table 2, Fig. 1), located in the northeastern area of Zhongguai uplift labeled as district III, some oils belong to group I, such as oil Ke94O1 with ON 45, some oils belong to group II, such as oils Ke301O1, MH1O1, JL1O1 and JTO1 with ON 46, 52, 53 and 54, respectively, and the remaining oils belong to mixtures of group I and II oils (Fig. 10f).

It is obvious that group I oils correlate with extracts of source rocks of the Lower Permian Fengcheng Formation (P$_{1f}$), while group II oils correlate with source rocks JT1S1, J23S3 and SS1S3 of Middle Permian age based on δ^{13}C values of individual *n*-alkanes and their variation with increasing carbon number (Fig. 10). δ^{13}C values of group I and II oil *n*-alkanes are relatively higher than extracts of source rocks of the Lower Permian Fengcheng Formation (P$_{1f}$) and Middle Permian age, respectively (Fig. 10a, d and e). This result can be mainly ascribed to a maturation effect as demonstrated by δ^{13}C variation of oil pyrolysates with increasing temperatures and EASY%Ro (Fig. 10b and c). Furthermore, among group I oils, oils FN4O1, FN7O1 and X87O1 with ON 5, 3 and 11, respectively have lower δ^{13}C values while oils
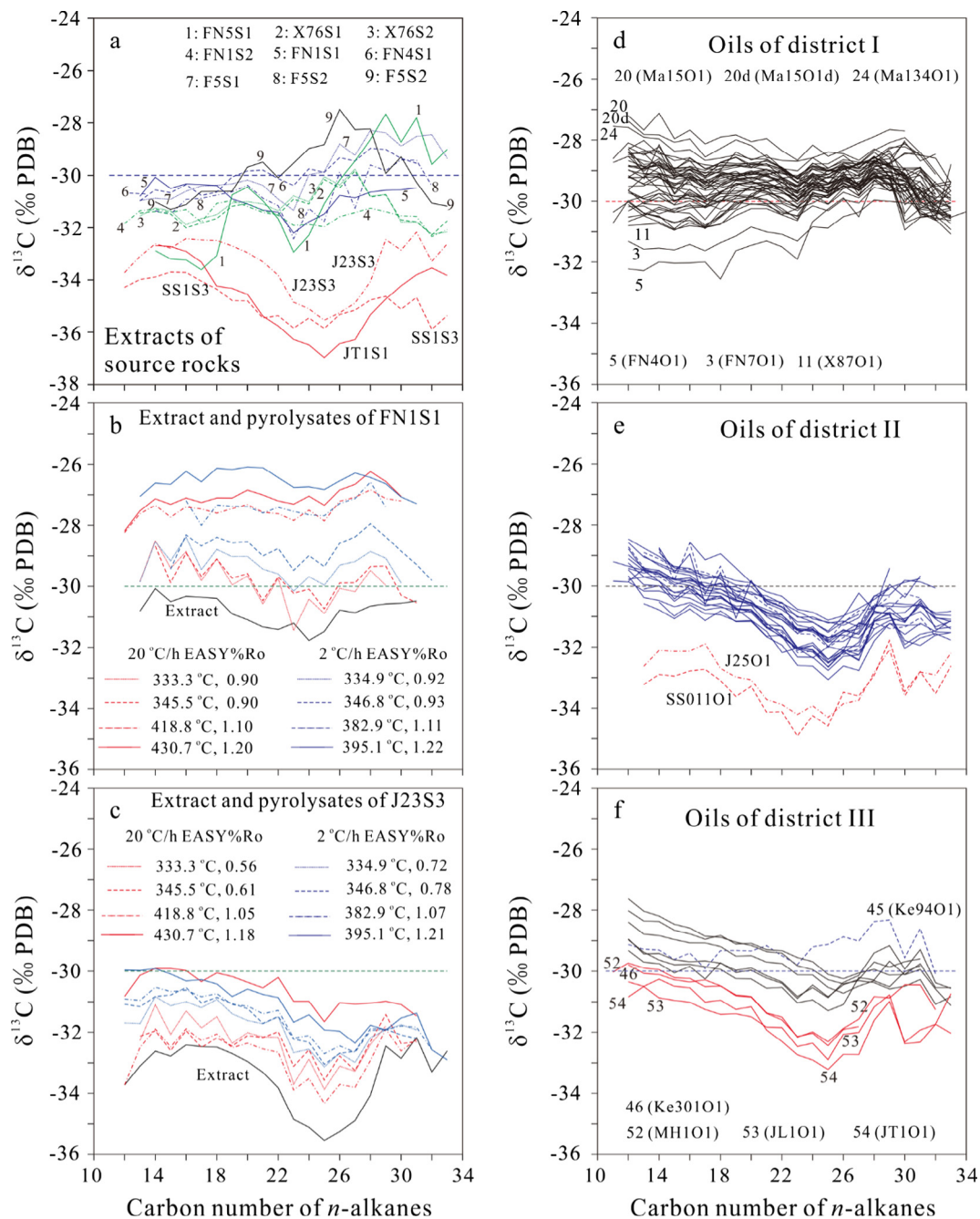
Fig. 10. δ^{13}C values of individual *n*-alkanes for the extracts and oil pyrolysates of source rocks and crude oils. (a): extracts of source rocks; (b): extract and oil pyrolysates for source rock FN1S1; (c): extract and oil pyrolysates for source rock J23S3; (d): oils in district I; (e): oils in district II; (f): oils in district III.

Ma15O1 and its duplicate Ma15O1d and Ma134O1 with ON 20 and 24, respectively have higher *n*-alkane δ^{13}C values. The former have substantially lower maturities with tricyclic terpanes/(tricyclic terpanes + C_{30} hopane) ratio ranging from 0.14 to 0.41 than the latter with this ratio ranging from 0.53 to 0.73 (Table 2, Fig. 10d).

Facies variation in the source rocks also substantially influence δ^{13}C values of individual *n*-alkanes. Source rock JT1S1 has a substantially higher maturity than source rocks J23S3 and SS1S3. However, the former has lower δ^{13}C values of individual *n*-alkanes than the latter (Fig. 10a). Oil JT1O1 has a higher maturity than most of the group II oils based on tricyclic terpanes/(tricyclic terpanes + C_{30} hopane) ratio and C_{29} steranes 20S/(20S + 20R) and $\alpha\beta\beta/(\alpha\alpha\alpha + \alpha\beta\beta)$ ratios (Table 2, Fig. 8), but this oil has the lowest *n*-alkane δ^{13}C values among group II oils (Fig. 10e and f). This result can be only ascribed to the variation in biological precursors in the source rocks.

5.2.2. Oil source correlation using molecular parameters

Group I oils in district I generally have higher Pr/*n*-C_{17} and Ph/*n*-C_{18} ratios and lower Pr/Ph ratio and correlate well to source rocks of the Fengcheng Formation (P_{1f}, Table 1 and 2, Figs. 4a, 5, and 7). Group II oils in district II generally have lower Pr/*n*-C_{17} and Ph/*n*-C_{18} ratios and higher Pr/Ph ratios and correlate with source rock JT1S1 of the Middle Permian Lower Wuerhe Formation (Tables 1 and 2, Figs. 4a, 6, and 8). Oil J25O1 has a higher Pr/*n*-C_{17} and Ph/*n*-C_{18} ratio, correlating with source rock J23S3 of the Middle Permian Lucaogou Formation (P_{2l}, Figs. 4a, 6d, and 9a). Oils HS4O1, HS6O1 and CF5O1 with ON 55, 57 and 67, respectively have higher Pr/*n*-C_{17} ratios (Table 2, Fig. 4a). In addition, oil HO15O1 with ON 61 has a Pr/*n*-C_{17} ratio of 6.30 (Table 2), which is not shown in Fig. 4a. All four oils were influenced by biodegradation as discussed later. Oils Ke301O1, MH1O1, JL1O1 and JTO1 in

district III with ON 46, 52, 53 and 54, respectively have lower Pr/n-C$_{17}$ and Ph/n-C$_{18}$ ratios and higher Pr/Ph ratios, belonging to group II oils (Table 2, Fig. 4a), consistent with carbon isotopic compositions (Fig. 10e and f). However, these three ratios overlap between group I and II oils. For example, Pr/n-C$_{17}$, Ph/n-C$_{18}$ and Pr/Ph ratios of group I oil X81O1 (ON 10) are 0.69, 0.61 and 1.32, within the ranges of these three ratios for group II oils (Table 2, Fig. 4a).

Group I oils generally have higher gammacerane/(C$_{30}$ hopane + gammacerane) and β-carotane/(β-carotane + C$_{30}$ hopane) ratios than group II oils (Table 2, Fig. 4b). The former correlate with source rocks of the Lower Permian Fengcheng Formation, while group II oils correlate with source rocks JT1S1, J23S3 and SS1S3 of Middle Permian age based on these two ratios. However, groups I and II oils have higher β-carotane/(β-carotane + C$_{30}$ hopane) ratios than the nine source rocks of the Fengcheng Formation and the three source rocks of Middle Permian age, respectively. This result could possibly be related to maturity differences. The oil samples, especially group I oils, have substantially higher maturity than the source rocks as demonstrated by the tricyclic terpanes/(tricyclic terpanes + C$_{30}$ hopane) ratio and C$_{29}$ steranes 20S/(20S + 20R) and αββ/(ααα + αββ) ratios (Tables 1 and 2, Fig. 4e and f). β-carotane may be more thermally stable than the C$_{30}$ hopane, and therefore, the β-carotane/(β-carotane + C$_{30}$ hopane) ratio increases with maturity (Table 2, Fig. 4b).

There is no clear difference between group I and II oils in Ts/(Tm + Ts), C$_{29}$Ts/(C$_{29}$ hopane + C$_{29}$Ts) and C$_{30}$ diahopane/(C$_{30}$ diahopane + C$_{30}$ hopane) ratios (Table 2 and Fig. 4c). This result can be ascribed to both facies and maturity variations in the source rocks. These three ratios are generally higher for group I oils than the nine source rocks of the Fengcheng Formation because the former have higher maturity than the latter.

Most oils of group II and in district III have tricyclic terpane distribution patterns with C$_{20}$ < C$_{21}$ and C$_{21}$ > C$_{23}$, similar to source rocks JT1S1, J23S3 and SS1S3 of Middle Permian age. This result is consistent with the studies by Wang and Kang (1999, 2001). However, five oils of this type, i.e. oils G28O1, G28O2, CP3O1, XY11O1 and J25O1 with ON 50, 51, 65, 74 and 77, respectively have C$_{20}$ < C$_{21}$ < C$_{23}$, inconsistent with this result (Table 2, Fig. 4d). Group I oils mainly have patterns of C$_{20}$ < C$_{21}$ < C$_{23}$ and C$_{20}$ > C$_{21}$ > C$_{23}$, with a few having C$_{20}$ > C$_{21}$ and C$_{21}$ < C$_{23}$, and C$_{20}$ < C$_{21}$ and C$_{21}$ > C$_{23}$ (Table 2, Fig. 4d). All group I oils which have C$_{20}$ > C$_{21}$ > C$_{23}$ have high maturity with a tricyclic terpanes/(tricyclic terpanes + C$_{30}$ hopane) ratio > 0.50 (Table 2).

Previous studies have demonstrated that the relative concentrations of tricyclic terpanes with lower carbon number increase and the distribution pattern of tricyclic terpanes changes from C$_{20}$ < C$_{21}$ < C$_{23}$ to C$_{20}$ > C$_{21}$ > C$_{23}$ with increasing maturity (Aquino Neto et al., 1983; Shi et al., 1988; Zhang et al., 2000, 2005; Pan et al., 2003; Zhang and Huang, 2005; Pan and Liu, 2009; Jia et al., 2010; P. Li et al., 2010; S. Li et al., 2010; Yu et al., 2011; Jin et al., 2014). It is possible that the distribution of tricyclic terpanes for group I oils changed from C$_{20}$ < C$_{21}$ < C$_{23}$ at lower maturity to C$_{20}$ > C$_{21}$ > C$_{23}$ at higher maturity. However, some group I oils which have high maturities with a tricyclic terpanes/(tricyclic terpanes + C$_{30}$ hopane) ratio > 0.50, even up to 0.91, have C$_{20}$ < C$_{21}$ < C$_{23}$ (Table 2). Therefore, the change from C$_{20}$ < C$_{21}$ < C$_{23}$ to C$_{20}$ > C$_{21}$ > C$_{23}$ is not the general route for tricyclic terpane maturation.

5.3. Oil biodegradation

Previous studies have reported biodegradation effects on oils in northwestern and central areas of Junggar Basin (e.g., Jiang et al., 1990; Pan et al., 2003). Four group II oils HS4O1, HS6O1, HO15O1 and CF5O1 with ON 55, 57, 61 and 67 collected from the southwestern area of Zhongguai uplift clearly suffered biodegradation.

Gas chromatograms, m/z 44 mass chromatogram from GC–IRMS and m/z 191 and m/z 217 mass chromatograms from GC–MS of oils HS6O1 and HO15O1 are shown in Fig. 11, while the chromatograms of oils HS4O1 and CF5O1 are not shown. Gas chromatograms for oils HS6O1 and CF5O1 show a pronounced unresolved complex mixture (UCM, Fig. 11a). Oils HS4O1 and HO15O1 have unusually high Pr/n-C$_{17}$ and Ph/n-C$_{18}$ ratios (Table 2, Figs. 4a and 11e). For oils HS6O1 and CF5O1, the initial oil components were severely biodegraded, resulting in complete removal of n-alkanes and acyclic isoprenoids for both oils, and even the removal of most C$_{27}$–C$_{29}$ regular steranes for oil HS6S1 (Fig. 11a–d). Later, these two initial oils were mixed with trace amounts of fresh oil components which were slightly biodegraded either before and/or after mixing. Therefore, these two oils contain trace amounts of n-alkanes and Pr and Ph (Fig. 11a and b). For oils HS4O1 and HO15O1, the whole oils appear to have suffered minor biodegradation, resulting in the partial removal of n-alkanes (Fig. 11e–h). All the four biodegraded oils have similar δ^{13}C values of individual n-alkanes and variations with carbon number to the non-biodegraded oils of group II (Fig. 10e).

5.4. Oil sources

The favorable source rocks within the Lower Permian Fengcheng Formation (P$_{1f}$) are located in the northern and central areas of Mahu sag while the effective source rocks within the Middle Permian Lower Wuerhe Formation (P$_{2w}$) occur in the southern areas of Mahu sag and the Sawan and Penyijingxi sags in the central Junggar Basin based on the variation of facies and thickness of source rocks within these two formations (Zhang et al., 1993; Cao et al., 2005, 2006). The occurrences of group I and II oils are consistent with the distributions of these two source rocks (Fig. 1). Group I oils appear exclusively derived from the source rocks within the Fengcheng Formation (P$_{1f}$), while group II oils were mainly derived from source rocks within the Lower Wuerhe Formation (P$_{2w}$) based on δ^{13}C values and trends of individual n-alkanes, in combination with molecular parameters (Figs. 4 and 10).

Previous studies have suggested that source rocks within the Fengcheng Formation (P$_{1f}$) are present over the whole Mahu sag and in the Penyijingxi and Sawan sags in the central Junggar Basin based on seismic data (e.g., Zhang et al., 1993; Cao et al., 2005). Sequential extraction and molecular analysis of fluid inclusions in oil-bearing reservoir rocks demonstrated that oil reservoirs in the central areas of Junggar Basin were derived from multiple source rocks of Permian age (Pan et al., 2003; Cao et al., 2005, 2006; Xiang et al., 2015). The result that δ^{13}C values of individual n-alkanes for group II oils are higher than the extract of source rock JT1S1 of the Lower Wuerhe Formation (P$_{2w}$) can be also ascribed to the mixing of oil components from source rocks of the Lower Wuerhe and Fengcheng formations, in addition to the effects of maturity and facies variations among source rocks within Lower Wuerhe Formation (Fig. 10). However, the phenomenon that n-alkane δ^{13}C values for group I oils are higher than the extracts of the nine source rocks of Fengcheng Formation (P$_{1f}$) can only be ascribed to maturity and facies variations among source rocks within the Fengcheng Formation (Fig. 10).

Oils in district III were derived from multiple source rocks within the Fengcheng and Lower Wuerhe formations based on δ^{13}C values of individual n-alkanes. Oil Ke94O1 (ON45) is typical of group I, and is derived from source rocks of the Fengcheng Formation. In contrast, oils Ke301O1, MH1O1, JL1O1 and JTO1 with ON 46, 52, 53 and 54, respectively are typical group II oils and have higher proportions of oil components derived from source rocks of the Lower Wuerhe Formation. The remaining oils in this district appear intermediate between these two groups (Figs. 1 and 10f). Biomarker compositions of oils in this district also show mixed
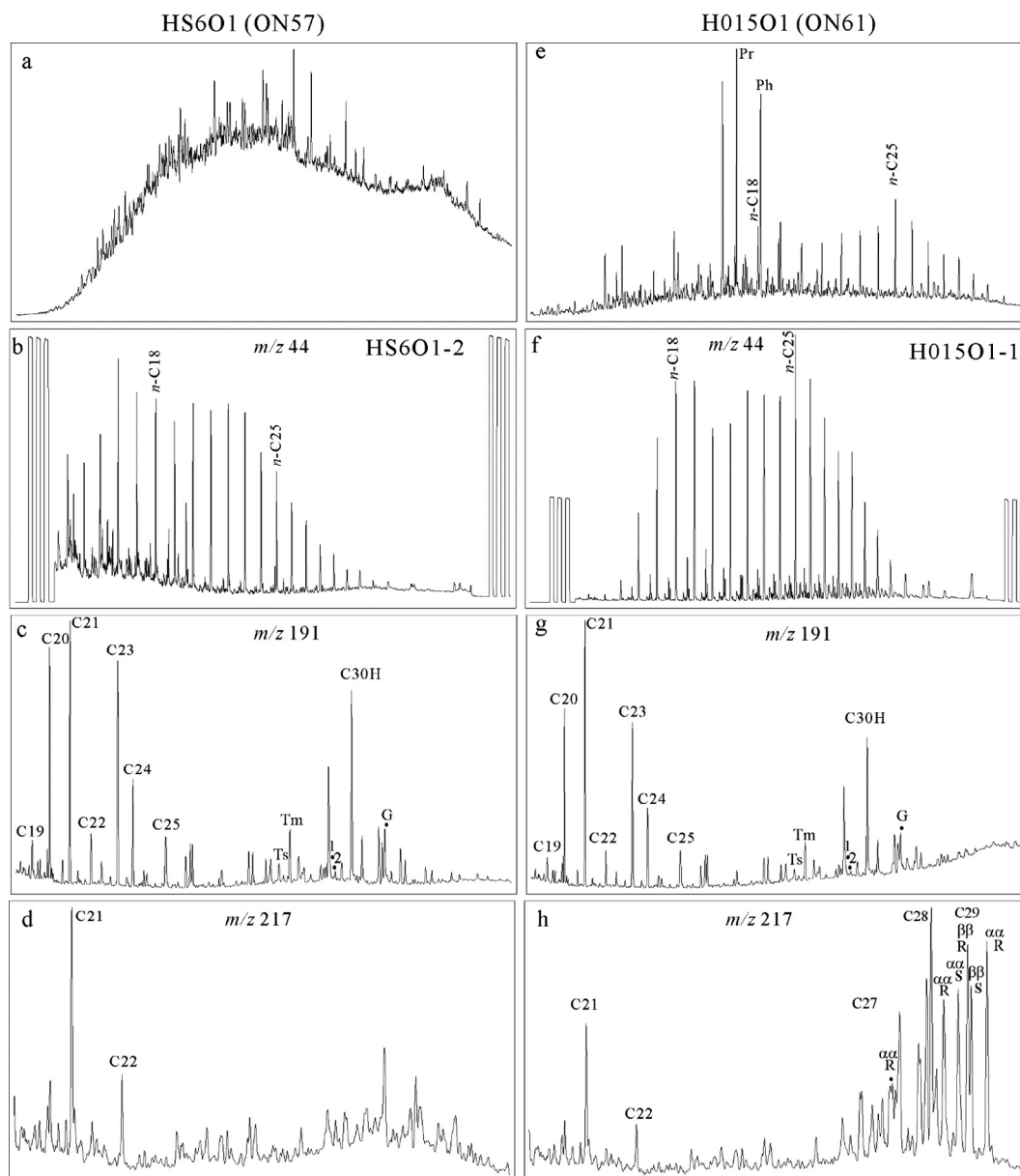
Fig. 11. Gas chromatograms and *m/z* 44 mass chromatograms for GC–IRMS and *m/z* 191 and *m/z* 217 mass chromatograms for GC–MS of biodegraded oils HS6O1 and H015O1 in district II. In (c) and (g), C19–C25: C$_{19}$ to C$_{25}$ tricyclic terpanes; 1: C$_{29}$Ts; 2: C$_{30}$ diahopane; G: gammacerane.

features. These oils have β-carotane/(β-carotane + C$_{30}$hopane) ratios closer to group I oils while they have the distribution pattern of tricyclic terpanes closer to group II oils (Fig. 4b and d).

It is noteworthy that oils were clearly derived from different source rocks and different source kitchens in the Xiayan uplift in the northeastern part of the studied area (Figs. 1 and 12). The eight oils with ON 27–34 in the western area of the uplift belong to group I and were derived from source rocks within the Fengcheng Formation in the Mahu sag west of the uplift, while the three oils with ON 74–76 in the eastern area of the uplift belong to group II and were derived from source rocks of both the Lower Wuerhe and Fengcheng formations in Penyijingxi sag, south of the uplift (Figs. 1 and 12).

Early studies suggested that source rocks within the Lower Permian Jiamuhe Formation (P$_1$j) below the Fengcheng Formation (P$_1$f) could be one of the major contributors of oils in the northwestern area (Yang et al., 1992; Zhang et al., 1993; Wang and Kang, 1999, 2001; Cao et al., 2005, 2006). Effective oil-prone source rock samples have not been obtained from this formation thus far. An oil source from this formation cannot be excluded. However, its contribution to oil reservoirs in the northwestern area is insignificant compared with source rocks within the Fengcheng and Lower Wuerhe formations.

6. Conclusions

The 78 oils can be clearly classified into two groups with substantial differences in δ^{13}C values of individual *n*-alkanes. For group I oils, the δ^{13}C values are relatively higher and remain stable with increasing carbon number. For group II oils, these values are relatively lower and decrease at first, to the lowest values at *n*-C$_{25}$, and then increase with carbon number. Differences in molecular parameters can be also observed between these two group oils. Group I oils generally have higher Pr/*n*-C$_{17}$ and Ph/*n*-C$_{18}$ ratios
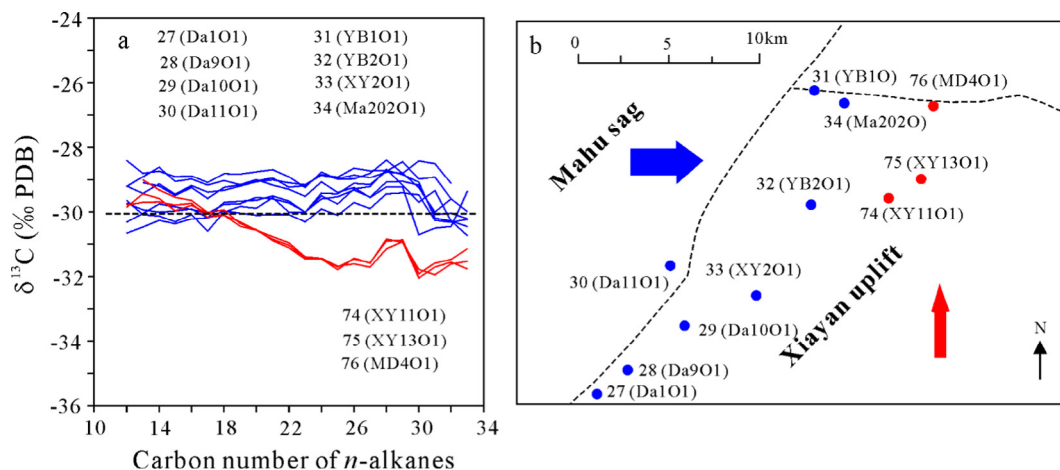
Fig. 12. $\delta^{13}C$ values of individual *n*-alkanes and origins for oils from the Xiayan uplift.

and lower Pr/Ph ratio, and higher gammacerane/(C$_{30}$ hopane + gammacerane) and β-carotane/(β-carotane + C$_{30}$ hopane) ratios, compared with group II oils. In addition, group I oils mainly have tricyclic terpane distribution patterns of C$_{20}$ < C$_{21}$ < C$_{23}$ and C$_{20}$ > C$_{21}$ > C$_{23}$ while group II oils mainly have the pattern of C$_{20}$ < C$_{21}$ and C$_{21}$ > C$_{23}$. However, molecular parameters overlap to some extent between these two groups of oils. Group I oils correlate well to source rocks of the Lower Permian Fengcheng Formation (P$_{1f}$), while group II oils correlate well to source rocks of Middle Permian age based on carbon isotopic and molecular compositions. The occurrences of these two groups of oils are well consistent with facies and thickness variations of source rocks within the Lower Permian Fengcheng Formation (P$_{1f}$) and Middle Permian Lower Wuerhe Formation (P$_{2w}$) in the northwestern and central Junggar Basin.

Acknowledgements

Associate Editor—**Andrew Murray**

References

Aquino Neto, F.R., Trendel, J.M., Restle, A., Connan, J., Albrecht, P.A., 1983. Occurrence and formation of tricyclic and tetracyclic terpanes in sediments and petroleums. In: Bjorøy, M., Albrecht, P., Cornford, C., de Groot, K., Eglinton, G., Galimov, E., Leythaeuser, D., Pelet, R., Rullkötter, J., Speers, G. (Eds.), Advances in Organic Geochemistry 1981. John Wiley & Sons, pp. 659–666.

Bjorøy, M., Hall, K., Gillyon, P., Jumeau, J., 1991. Carbon isotope variations in *n*-alkanes and isoprenoids of whole oils. Chemical Geology 93, 13–20.

Bjorøy, M., Hall, P.B., Hustad, E., Williams, J.A., 1992. Variation in stable isotope ratios of individual hydrocarbons as a function of artificial maturity. Organic Geochemistry 19, 89–105.

Bjorøy, M., Hall, P.B., Moe, R.P., 1994. Variation in the isotopic composition of single components in the C$_4$–C$_{20}$ fraction of oil and condensates. Organic Geochemistry 21, 761–776.

Cao, J., Zhang, Y., Hu, W., Yao, S., Wang, X., Zhang, Y., Tang, Y., 2005. The Permian hybrid petroleum system in the northwest margin of the Junggar Basin, NW China. Marine and Petroleum Geology 22, 331–349.

Cao, J., Yao, S.P., Jin, Z.J., Hu, W.X., Zhang, Y.J., 2006. Petroleum migration and mixing in the northwestern Junggar Basin (NW China): constraints from oil-bearing fluid inclusion analyses. Organic Geochemistry 37, 827–846.

Carrol, A.R., Brassell, S.C., Graham, S.A., 1992. Upper Permian lacustrine oil shales, southern Junggar basin, northwest China. American Association of Petroleum Geologists Bulletin 76, 1874–1902.

Carroll, A.R., 1998. Upper Permian lacustrine organic facies evolution, southern Junggar Basin, NW China. Organic Geochemistry 28, 649–667.

Chen, G., Ablimit, Bai, L., Zhang, J., Bian, B., 2013. Petroleum accumulation field in the deep strata of the eastern slope area of the Mahu Sag, Junggar Basin. Journal of Southwest Petroleum University: Science & Technology Edition 35 (6), 31–38 (in Chinese).

Chen, G., An, Z., Abulimiti, Li, X., Xu, Q., Zhang, L., 2014. Petroleum exploration prospects of Carboniferous-Permian in peripheral Mahu Sag, Junggar Basin. Xinjiang Petroleum Geology 35, 259–263 (in Chinese).

Chen, J., Liang, D., Wang, X., Zhong, N., Song, F., Deng, C., Shi, X., Jin, T., Xiang, S., 2003. Mixed oils derived from multiple source rocks in the Cainan oilfield, Junggar Basin, northwest China. Part I: Genetic potential of source rocks, features of biomarkers and oil sources of typical crude oils. Organic Geochemistry 34, 889–909.

Clayton, C.J., 1991. Effect of maturity on carbon isotope ratios of oils and condensates. Organic Geochemistry 17, 887–899.

Clayton, C.J., Bjorøy, M., 1994. Effect of maturity on $^{12}C/^{13}C$ ratios of individual compounds in North Sea oils. Organic Geochemistry 21, 737–750.

Clayton, J.L., Yang, J., King, J.D., Lillis, P.G., Warden, A., 1997. Geochemistry of oils from the Junggar Basin, Northwest China. Association of Petroleum Geologists Bulletin 81, 1926–1944.

Collister, J.W., Summons, R.E., Lichtfouse, E., Hayes, J.M., 1992. An isotopic biogeochemical study of the Green River oil shale. Organic Geochemistry 19, 265–276.

Collister, J.M., Lichtfouse, E., Hieshima, G., Hayes, J.M., 1994. Partial resolution of source of n-alkanes in the saline portion of the Parachute Creek Member, Green River Formation (Piceance Creek Basin, Colorado). Organic Geochemistry 21, 645–659.

Eglinton, T.I., 1994. Carbon isotopic evidence for the origin of macromolecular aliphatic structures in kerogen. Organic Geochemistry 21, 721–735.

Freeman, K.H., Hayes, J.M., Trendel, J.M., Albrecht, P., 1990. Evidence from carbon isotope measurements for diverse origins of sedimentary hydrocarbons. Nature 343, 254–256.

Gao, G., Wang, X., Liu, G., Zhang, Y., Huang, Z., 2012. Analyses of the genesis and potential of natural gas in Kebai area of Northwest Margin, Junggar Basin. Geological Journal of China Universities 18 (2), 307–317 (in Chinese).

Graham, S.A., Brassell, S.C., Carroll, A.R., Xiao, X., Demaison, G., McKnight, C.L., Liang, Y., Chu, J., Hendrix, M.S., 1990. Characteristics of selected petroleum- source rocks, Xinjiang Uygur Autonomous Region, northwest China. American Association of Petroleum Geologists Bulletin 74, 493–512.

Hayes, J.M., Takigiku, R., Ocampo, R., Callot, H.J., Albrecht, P., 1987. Isotopic compositions and probable origins of organic molecules of the Eocene Messel shale. Nature 329, 48–51.

Hayes, J.M., Freeman, K.H., Popp, B.N., Hoham, C.H., 1990. Compound-specific isotopic analyses: a novel tool for reconstruction of ancient biochemical processes. Organic Geochemistry 16, 1115–1128.

Hill, R.J., Tang, Y., Kaplan, I.R., 2003. Insight into oil cracking based on laboratory experiments. Organic Geochemistry 34, 1651–1672.

Jia, X., Mai, G., Kuang, J., Wu, G., 1992. Characteristics of petroleum geology and hydrocarbon prospective analysis in the central area of Junggar Basin. In: Luo, B.

(Ed.), Petroleum Geology of the Junggar Basin. Gansu Science and Technology Press, pp. 234–245 (in Chinese).

Jia, W., Xiao, Z., Yu, C., Peng, P., 2010. Molecular and isotopic compositions of bitumens in Silurian tar sands from the Tarim Basin, NW China: Characterizing biodegradation and hydrocarbon charging in an old composite basin. Marine and Petroleum Geology 27, 13–25.

Jia, W., Wang, Q., Peng, P., Xiao, Z., Li, B., 2013. Isotopic compositions and biomarkers in crude oils from the Tarim Basin: oil maturity and oil mixing. Organic Geochemistry 57, 95–106.

Jiang, Z., Fan, G., 1983. Organic geochemistry of source rocks within Carboniferous Fengcheng Formation in Junggar Basin. Xinjiang Petroleum Geology 3 (3), 74–91 (in Chinese).

Jiang, Z., Fowler, M.G., 1986. Carotenoid-derived alkanes in oils from northwestern China. Organic Geochemistry 10, 831–839.

Jiang, Z., Philp, R.P., Lewis, C.A., 1988. Identification of novel bicyclic alkanes from steroid precursors in crude oils from Kelamayi Oilfield of China. Geochimica et Cosmochimica Acta 52, 491–498.

Jiang, Z., Fowler, M.G., Lewis, C.A., Philp, R.P., 1990. Polycyclic alkanes in a biodegraded oil from the Kelamayi oilfield, northwestern China. Organic Geochemistry 15, 35–46.

Jin, X., Pan, C., Yu, S., Li, E., Wang, J., Fu, X., Qin, J., Xie, Z., Zheng, P., Wang, L., Chen, J., Tan, Y., 2014. Organic geochemistry of marine source rocks and pyrobitumen-containing reservoir rocks of the Sichuan Basin and neighboring areas, SW China. Marine and Petroleum Geology 56, 147–165.

King, J.D., Yang, J., Fan, P., 1994. Thermal history of the periphery of the Junggar Basin, northwestern China. Organic Geochemistry 21, 393–405.

Li, E., Pan, C., Yu, S., Jin, X., Liu, J., 2013. Hydrocarbon generation from coal, extracted coal and bitumen-rich coal in confined pyrolysis experiments. Organic Geochemistry 64, 58–75.

Li, P., Feng, J., Lu, Y., Hao, F., Qi, J., Jiao, Y., Zhang, Z., Chen, H., 2010. Tectonic, Sedimentation and Petroleum Formation in Junggar Basin. Chinese Geological Publishing House, pp. 1–340 (in Chinese).

Li, S., Pang, X., Jin, Z., Yang, H., Xiao, Z., Gu, Q., Zhang, B., 2010. Petroleum source in the Tazhong Uplift, Tarim Basin: new insights from geochemical and fluid inclusion data. Organic Geochemistry 41, 531–553.

Li, X., Zha, M., Wu, K., 2007. Geochemical feature of natural gas in Wu-Xia area, Junggar Basin. Xinjiang Petroleum Geology 28, 413–415 (in Chinese).

Liu, B., Liu, D., Guo, T., Huang, Z., Liu, Z., Wu, F., 2013. Oil accumulation related to migration of source kitchens in northwestern margin structural belt, Junggar Basin. Petroleum Geology and Experiment 35, 621–625 (in Chinese).

Liu, B., He, B., Huang, Z., Zhang, Y., Yin, Z., Guo, T., Wu, F., 2014. Sources and distribution patterns of natural gas of different genetic types at the northwestern margin of the Junggar Basin. Natural Gas Industry 34 (9), 40–46 (in Chinese).

Love, G.D., Snape, C.E., Fallick, A.E., 1998. Differences in the mode of incorporation and biogenicity of the principal constituents of a type I oil shale. Organic Geochemistry 28, 797–811.

Odden, W., Barth, T., Talbot, M.R., 2002. Compound-specific carbon isotope analysis of natural and artificially generated hydrocarbons in source rocks and petroleum fluids from offshore Mid-Norway. Organic Geochemistry 33, 47–65.

Pan, C., Yang, J., 2000. Geochemical characteristics and implications of hydrocarbons in reservoir rocks of Junggar Basin, China. Chemical Geology 167, 321–335.

Pan, C., Yang, J., Fu, J., Sheng, G., 2003. Molecular correlation of free oil and inclusion oil of reservoir rock in the Junggar Basin, China. Organic Geochemistry 34, 357–374.

Pan, C., Liu, D., 2009. Molecular correlation of the free oil, adsorbed oil and inclusion oil of reservoir rocks in the Tazhong Uplift of the Tarim Basin, China. Organic Geochemistry 40, 387–399.

Peters, K.E., Walters, C.C., Moldowan, J.M., 2005. The Biomarker Guide. Biomarkers and Isotopes in Petroleum Exploration and Earth History, vol. 2. Cambridge University Press, UK.

Ruble, T.E., Bakel, A.J., Philp, R.P., 1994. Compound specific isotopic variability in Uinta Basin native bitumens: paleoenvironmental implications. Organic Geochemistry 21, 661–671.

Schoell, M., Hwang, R.J., Carlson, R.M.K., Welton, J.E., 1994. Carbon isotopic composition of individual biomarkers in gilsonites (Utah). Organic Geochemistry 21, 673–683.

Shi, J., Wang, B., Zhang, L., Hong, Z., 1988. Study on diagenesis of organic matter in immature rocks. Organic Geochemistry 13, 869–874.

Song, Y., 1995. Geological Characteristics of Gas Accumulation Belts in the Junggar Basin. Petroleum Industry Press, Beijing (in Chinese).

Sweeney, J.J., Burnham, A.K., 1990. Evaluation of a simple model of vitrinite reflectance based on chemical kinetics. American Association of Petroleum Geologists Bulletin 74, 1559–1570.

Wang, X., Gao, G., Yang, H., Liu, G., Huang, Z., Wei, H., 2008. Research on relation between oil properties and petroleum pool formation of Permian in the 5th & 8th districts, northwestern margin of Junggar Basin. Geological Journal of China Universities 14, 256–261 (in Chinese).

Wang, X., Kang, S., 1999. Analysis of crude origin in hinterland and slope of northwest margin. Junggar Basin. Xinjiang Petroleum Geology 20 (2), 108–112 (in Chinese).

Wang, X., Kang, S., 2001. On the oil source of the Mabei oil field, northwest Junggar Basin. Journal of Southwest Petroleum Institute 23 (6), 6–8 (in Chinese).

Wang, X., Zhi, D., Wang, Y., Chen, J., Qin, Z., Liu, D., Xiang, Y., Lan, W., Li, N., 2013. Source Rocks and Oil-Gas Geochemistry in Junggar Basin. Chinese Petroleum Industry Press (in Chinese).

Wilhelms, A., Larter, S.R., Hall, K., 1994. A comparative study of the stable carbon isotopic composition of crude oil alkanes and associated crude oil asphaltene pyrolysate alkanes. Organic Geochemistry 21, 751–759.

Xiang, B., Zhou, N., Ma, W., Wu, M., Cao, J., 2015. Multiple-stage migration and accumulation of Permian lacustrine mixed oils in the central Junggar Basin (NW China). Marine and Petroleum Geology 59, 187–201.

Xiang, B., Li, E., Gao, X., Wang, M., Wang, Y., Xu, H., Huang, P., Yu, Y., Liu, J., Zou, Y., Pan, C., 2016. Petroleum generation kinetics for Permian lacustrine source rocks in the Junggar Basin, NW China. Organic Geochemistry 98, 1–17.

Xiong, Y., Geng, A., 2000. Carbon isotopic composition of individual n-alkane in asphaltene pyrolysates of biodegraded crude oils from the Liaohe Basin, China. Organic Geochemistry 31, 1441–1449.

Yang, B., Ma, Q., Gan, Z., 1985. Thermal evolution of organic matter and petroleum generation threshold of Aican-1 well. Oil & Gas Geology 6 (4), 379–385 (in Chinese).

Yang, B., Jiang, Z., Li, J., Wang, X., 1992. Origins of petroleum in northwestern Junggar Basin. In: Luo, B. (Ed.), Petroleum Geology of the Junggar Basin. Gansu Science and Technology Press, pp. 62–73 (in Chinese).

Yu, S., Pan, C., Wang, J., Jin, X., Jiang, L., Liu, D., Lü, X., Qin, J., Qian, Y., Ding, Y., Chen, H., 2011. Molecular correlation of crude oils and oil components from reservoir rocks in the Tazhong and Tabei uplift of the Tarim Basin, China. Organic Geochemistry 42, 1241–1262.

Yu, S., Pan, C., Wang, J., Jin, X., Jiang, L., Liu, D., Lü, X., Qin, J., Qian, Y., Ding, Y., Chen, H., 2012. Correlation of crude oils and oil components from reservoirs and source rocks using carbon isotopic compositions of individual n-alkanes in the Tazhong and Tabei Uplift of the Tarim Basin, China. Organic Geochemistry 52, 67–80.

Yu, S., Wang, X., Xiang, B., Liao, J., Wang, J., Li, E., Yan, Y., Cai, Y., Zou, Y., Pan, C., 2014. Organic geochemistry of Carboniferous source rocks and their generated oils from the Eastern Junggar Basin, NW China. Organic Geochemistry 77, 72–88.

Zhang, G., Wang, Z., Wu, M., Wu, Q., Yang, B., Yang, W., Yang, R., Fan, G., Zheng, D., Zhao, B., Peng, X., Yong, T., 1993. Petroleum geology of Junggar Basin. In: Zhai, G. (Ed.), Petroleum Geology of China, vol. 15. Chinese Petroleum Industrial Press, pp. 1–390 (in Chinese).

Zhang, S., Hanson, A.D., Moldowan, J.M., Graham, S.A., Liang, D., Chang, E., Fago, F., 2000. Paleozoic oil–source rock correlations in the Tarim Basin, NW China. Organic Geochemistry 31, 273–286.

Zhang, S., Huang, H., 2005. Geochemistry of Palaeozoic marine petroleum from the Tarim Basin, NW China: Part 1. Oil family classification. Organic Geochemistry 36, 1204–1214.

Zhang, S., Huang, H., Xiao, Z., Liang, D., 2005. Geochemistry of Paleozoic marine petroleum from the Tarim Basin, NW China. Part 2: Maturity assessment. Organic Geochemistry 36, 1215–1225.

Zhao, B., 1992a. Nature of basement of Junggar Basin. Xinjiang Petroleum Geology 13 (2), 95–99 (in Chinese).

Zhao, B., 1992b. Formation and evolution of Junggar Basin. Xinjiang Petroleum Geology 13 (3), 191–196 (in Chinese).

Zhou, Z., Sheng, G., Sheng, R., Ming, Y., Lin, M., Zhang, H., Song, M., 1989. Petroleum Geochemistry of Junggar Basin, China. Chinese Science Press, pp. 1–74 (in Chinese).